Hydrogel-forming microneedles for rapid and efficient skin deposition of controlled release tip-implants

Ke Peng, Lalitkumar K. Vora, Juan Domínguez-Robles, Yara A. Naser, Mingshan Li, Eneko Larrañeta, Ryan F. Donnelly

Affiliation/s School of Pharmacy, Queen's University Belfast, Medical Biology Centre, 97 Lisburn Road, Belfast BT9 7BL, UK

Corresponding author information: R.Donnelly@qub.ac.uk (R.F. Donnelly)

Abstract

In this work, we introduce, for the first time, novel hybrid microneedle patches with implantable poly(lactic-co-glycolic acid) (PLGA) tips aligned with hydrogel-forming microneedle bases (HFMB) using a dissolvable material. A model dye, Nile red, and an antifungal drug, amphotericin B, were loaded into the PLGA tips in a controlled manner by multiple castings. Three different types of pre-formed microneedle bases including conventional dissolving baseplates (MN0), HFMB with needle heights of 600 µm (MN6) and HFMB with needle heights of 800 µm (MN8) were investigated. Compared to the conventional dissolving baseplate (MN0)-based PLGA tipped implantable microneedle design, the addition of the pre-formed HFMB (MN8) improved *in vitro* and *ex vivo* insertion capacities of the patches, increased *ex vivo* drug delivery efficiency up to 80% of the loaded drug and speeded up the implantation process to within one minute. An adhesion test indicated that the hydrogel baseplate used in this study was easier to peel off from the skin than the dissolving baseplate. *In vitro* release studies demonstrated that the release of amphotericin B from the drug loading PLGA tips lasts for a week. Antifungal tests of the inserted amphotericin B loaded PLGA tips revealed their antifungal effects against *Candida albicans*. The MN8 did not dissolve, leaving no viscous residue but absorbed water and disintegrated after immersion into water. The hybrid PLGA-tipped microneedle system will be ideal for rapid implantation and sustained release of amphotericin B for dermal fungal infections. This hybrid patch design is a novel promising technology for delivering drug-eluting microimplants into the skin while ensuring easy and complete removal of the HFMB. It could have many potential applications in implantable intradermal drug delivery.

Keywords: Implantable microneedles, fast separable microneedles, intradermal delivery, sustained release, amphotericin B

1. Introduction

Implant devices or long-acting formulations are generally inserted/injected into the body subcutaneously or into a body cavity with the aid of surgery, or by using a special needle [1,2] procedures often leave a wound and bleeding usually ensues to some extent. Such invasive procedures are not usually able to be administered outside of professional healthcare [3]. In order to address these limitations, microneedle patches may be used to administer long-acting formulations [4].

Microneedle patches are minimally invasive devices capable of bypassing the outermost layer of the skin (*stratum corneum*) allowing the delivery of a wide variety of active compounds into and through the skin [5–7]. These devices are formed by arrays of microprojections with lengths ranging from a few microns up to 1-2 mm [8,9]. Microneedle patches have great potential to enable patients to self-administer therapies otherwise requiring hypodermic injections with the use of a simple transdermal patch-like device [10]. Interest in the applications of microneedle devices is growing, as they could provide a patient-friendly option to overcome several long-standing clinical problems including complications associated with device implantation [4]. Several strategies have been developed to achieve this, such as loading long-acting particulate systems within the microneedle tips [4,11,12] or loading drugs with biodegradable polymers, such as poly(lactic-co-glycolic acid) (PLGA), to form implantable tips capable of providing a sustained release profile [13]. The latter type of microneedle patches needs to be carefully designed. Pedestals capable of dissolving after insertion are used to connect the biodegradable tips with the baseplate. In this way, the implantable microneedle tips will be left inside the skin after insertion. Most researchers chose dissolving materials as the baseplate and also to fill the space between the tips and the baseplate [13–15]. This strategy requires complete dissolution of the pedestals, thus requiring a relatively long time. Furthermore, dissolution of the dissolving baseplate would leave a viscous gel on the skin surface of the patients, which are adhesive to and hard to peel off from the skin surfaces, posing the risk of dragging the tips out of the skin upon removal. Importantly, such a system requires excellent insertion capacities to implant the tips in skin, which limit their wide application [16]. Accordingly, there is a clear need to improve the design of the systems to allow a quick and easy implantation process as well as high efficiency.

This work aims to develop a microneedle patch system that can deliver tip-implants rapidly and efficiently. For this purpose, we propose the use of hydrogel-forming microneedles (HFMB), for the first time, as a shaft base for implantation of the PLGA microneedle tips. First reported in 2012, HFMB have been widely investigated as the newest form of microneedles [17,18]. They are unique in their ability to absorb water without dissolving themselves, leaving

no viscous residue on the skin surface when inserted into the skin. Furthermore, synthetic, tough hydrogels are generally not adhesive [19]. Microneedle patches fabricated from hydrogel-forming materials have shown to be a mechanically strong vehicle able to pierce the skin and thus could provide extra support for PLGA tip insertion [20]. Besides, the aligning of HFMB with PLGA tips reduces the amount of the dissolving material needed to fully fill the gap between the PLGA tips and the baseplate. In this way after insertion into the skin, the quick dissolution of the pedestals will allow rapid PLGA tips separation. Implantable microneedle tips were prepared using PLGA and two model compounds (Nile red and amphotericin B). The resulting patches were characterized by evaluating the efficacy of insertion and drug delivery.

2. Materials and methods

2.1. Materials

Amphotericin B was purchased from Cayman Chemical Company (purity specification ≥ 95%), (Ann Arbor, MI, USA). Nile red was obtained from Thermo Fisher Scientific (Waltham, Massachusetts, USA). Poly(lactic-co-glycolic acid) (PLGA), a 50:50 molar ratio of lactide: glycolide, the inherent viscosity of 0.55 – 0.75 dL/g was obtained from Lactel® (Birmingham, AL, USA). Plasdone™ K-29/32 (poly(vinylpyrrolidone), PVP, MW 58 kDa) was donated by Ashland, Kidderminster, UK. Poly(ethylene glycol) (PEG, molecular weight 200 Da) was purchased from Sigma-Aldrich (St. Louis, Missouri, USA). Gantrez® S-97, a copolymer of methyl vinyl ether and maleic acid (PVME/MA), with a molar mass of 1,200,000 Da was donated by Ashland (Kidderminster, UK).Plasdone® K-90D (MW = 360,000 Da), was provided by Ashland (Covington, Kentucky, USA). Parafilm M®, a flexible thermoplastic sheet (126 μm thickness) made of olefin-type material and used as a skin simulant for insertion studies [21], was purchased from Bemis Company (Neenah, Wisconsin, USA). Phosphate buffered saline (PBS) pH 7.4 tablets were obtained from Oxoid Limited (Hampshire, UK). Ethylenediaminetetraacetic acid disodium salt dehydrate (Na_2EDTA) and dodecyl sodium sulfate (SLS) were supplied by Sigma-Aldrich (Dorset, UK). 2,2,2-trifluoroethanol, also known as TFE was obtained from Fluorochem (Hadfield, Old Glossop, UK). Dimethyl sulfoxide (DMSO) was provided by VWR International Limited (Leicestershire, UK). HPLC-grade methanol, acetonitrile, and tetrahydrofuran (THF) were obtained from Sigma-Aldrich, Dorset, UK. All reagents were of analytical grade unless otherwise stated.

2.2 Fabrication of Nile red PLGA-tipped microneedle patches

To fabricate these hybrid patches, the Nile red PLGA tips and the bases were fabricated separately and then aligned together, as illustrated in Figure 1.

2.2.1 Fabrication of Nile red PLGA microneedle tips

Nile red PLGA tips were cast using silicone micromoulds (11 × 11 conical microneedle cavities on an 86 mm^2 area, 600 μm needle height, 300 μm in base diameter with a 600 μm interspacing, as summarised in Table 1). The tip solution for casting Nile red PLGA microneedle tips was prepared by dissolving 1 g PLGA pellets and 5.2 mg Nile red into 10 mL of a TFE and water mixture (90%: 10%, v/v). An aliquot of 20 μL tip solution was cast on the silicone moulds and centrifuged at 4472 × g for 10 min. The casting process was performed 1, 2, 3, or 4 times to fabricate C1, C2, C3, or C4 tips, respectively (Figure 1). The moulds with tips were placed in a vacuum oven (Jeio Tech, Seoul, Korea) overnight to remove the residue solvent.

2.2.2 Fabrication of the base of PLGA-tipped microneedle patches

Three different bases for microneedle patches (MN0, MN6, and MN8) were prepared and evaluated in this paper. The moulds for casting MN0 were silicone moulds with no holes (as detailed in Table 1). The moulds for casting MN6 were silicone moulds with conical holes in an 11 × 11 array (600 μm in height, 300 μm in base diameter, with a 600 μm interspacing, as summarised in Table 1), the same as those used for casting the PLGA microneedle tips. The moulds for casting MN8 were silicone moulds with an 11 × 11 array of conical holes (800 μm in height, 300 μm in width, and interspacing of 600 μm, as summarised in Table 1). The parameters of all the moulds used in this work are summarized in Table 1. The differences among MN0, MN6 and MN8 were the lengths of the needles, 0 for MN0, 600 μm for MN6 and 800 μm for MN8.

Table 1. Geometries of the moulds used for the base and the PLGA tips fabrication.

Moulds		Height (μm)	Width (μm)	Interspacing (μm)	Array
PLGA tips	MN6	600	300	600	11 × 11
Base	MN0	0	0	0	0
	MN6	600	300	600	11 × 11
	MN8	800	300	600	11 × 11

To fabricate Nile red PLGA-tipped microneedle patches, all the bases were prepared beforehand. For MN0, an aqueous gel (dissolving base gel) containing 15% w/w Plasdone® K-90D and 1.5% w/w glycerol was formulated. For MN6 and MN8, an aqueous gel (HFMB gel)

containing 25% w/w Gantrez® S-97 and 10% w/w PEG 200 Da was prepared. The base was prepared by casting 0.4 g of the gels into the corresponding moulds. The moulds loaded with the gel were centrifugated at 4472 × g for 10 min to fill the cavities and remove bubbles. The gel loaded in the mould was then dried at room temperature for 48 h. For MN6 and MN8, the dry HFMB gel was heated at 80ºC for 24 h to induce chemical crosslinking between Gantrez® S-97 and PEG *via* ester formation. The bases were sometimes trimmed to remove excess side walls without touching the needles.

2.2.3 Alignment of PLGA-tipped microneedle patches

The Nile red PLGA-tipped microneedle patches were then fabricated by aligning the base and the Nile red PLGA tips. An aqueous solution of 40% w/w PVP was cast on the moulds with Nile red PLGA tips inside. Centrifugation at 4472 × g was applied for 5 min. The excess PVP solution was immediately removed and a pre-formed base was aligned carefully by applying gentle manual force (Figure 1).

2.3. Fabrication of amphotericin B PLGA-tipped microneedle patches

Amphotericin B PLGA-tipped microneedle patches were fabricated following the same approach and using the same moulds as explained previously for the Nile red PLGA-tipped microneedle patches, with the exception of the formulation of the tip solution. The tip solution for casting amphotericin B PLGA tips was made up of 75 mg amphotericin B and 25 mg PLGA dissolved in 1 mL of DMSO. The casting procedure was conducted once, twice or three times to form C1, C2, or C3 tips, respectively. Prior to each casting procedure, the residue solvent was removed by placing the tips under the fume hood for 4 hours. Each part of this hybrid system, namely the bases and amphotericin B PLGA tips, were fabricated separately. Following their fabrication, the tips and the bases were then aligned together as illustrated in Figure 1. The bases used for amphotericin B PLGA-tipped microneedle patches were MN0, MN6, and MN8, the same as those used for Nile red PLGA-tipped microneedle patches, as detailed in section 2.2.2. Moreover, the base was aligned with amphotericin B PLGA tips as described in section 2.2.3 (Figure 1).

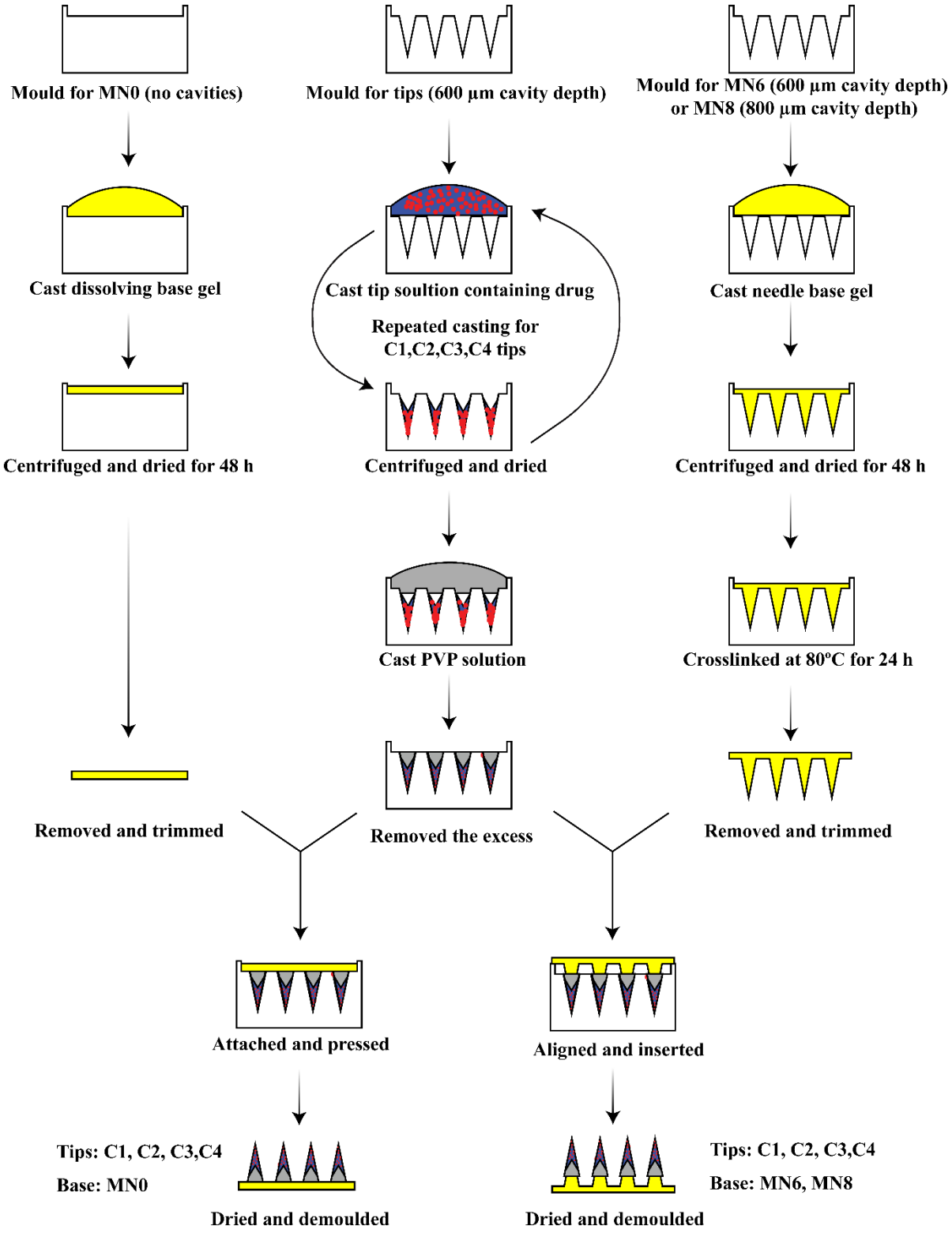

Figure 1. Schematic illustration of the microneedle patches' fabrication process. Different tip solutions were used for preparing different drug-containing tips. For fabricating Nile red PLGA-tipped microneedle patches, the tip solution was formulated with 0.1% w/v PLGA with 0.00052% w/v Nile red in TFE and water (9:1, v/v). For amphotericin B PLGA-tipped microneedle patches, the tip solution contained 7.5% w/v amphotericin B and 2.5% w/v PLGA in DMSO.

2.4 Insertion capabilities of microneedle patches in skin models

In vitro insertion performance of the resulting microneedle patches was evaluated using two models: Parafilm M® and full-thickness neonatal porcine skin. In the first case, sheets of Parafilm M® were folded to produce an eight-layer film with a thickness of 1 mm [22]. The insertion performance of various microneedle patches was examined using a Texture Analyzer TA XT-Plus (Stable Micro Systems, Surrey, UK) as described previously [23]. Briefly, the equipment was set in compression mode (pre-test and post-test speeds were 0.5 mm/s), the force was set at 32 N and the test was run for 30 s. In addition, the trigger force was set at 0.049 N. The patch was compressed at 32 N into the eight layers of folded Parafilm M® for 30 s. The inserted microneedle patch was then carefully removed from the Parafilm M® layers. Parafilm M® layers were unfolded and the number of holes in each layer was counted using a Leica EZ4 D stereo light microscope (Leica Microsystems, Milton Keynes, UK) equipped with two polarizing filters. The percentage of the created holes was presented as the ratio of the number of the holes created in each layer to the number of the needles of each array (121). The number of holes created in different Parafilm M® layers was used as an indication of the insertion depth as one layer of Parafilm M® layer has a thickness of 126 μm.

Full-thickness neonatal porcine skin (obtained from stillborn piglets) was used as a skin model for *ex vivo* insertion studies due to its similarities to human skin in general structure and physical properties [24]. Stillborn piglets were frozen at -20ºC immediately after birth and defrosted overnight before skin removal. The thickness of the skin was roughly 1 mm, as confirmed by a digital Vernier calliper micrometre. Skin samples were shaved and equilibrated in PBS (pH 7.4) for 30 min at 37°C to mimic the true physical conditions of human skin. Patches aligned with MN0, including Nile red PLGA-tipped microneedle patches C4-MN0 and C2-MN0, or amphotericin B PLGA-tipped microneedle patches C3-MN0, were manually inserted into the skin by applying firm pressure with a thumb for 3 min and kept in place for 30 min in total. A cylindrical stainless-steel weight (diameter 11.0 mm, 12.0 g mass) was placed on top of these patch to ensure microneedle insertion and to prevent microneedle expulsion. Patches aligned with MN6 and MN8, including Nile red PLGA-tipped microneedle patches C2-MN6 and C2-MN8, or amphotericin B PLGA-tipped microneedle patches C3-MN6 and C3-MN8 were manually inserted into skin samples by applying firm pressure with a thumb for 30 s and removed immediately afterwards. Following this, an optical coherence tomography (OCT) microscope EX1201 (Michelson Diagnostics Ltd., Kent, UK), was used to investigate the insertion process of microneedle patches in-skin, as detailed in our previous studies [25,26]. The 2D images were examined using the imaging software ImageJ® (National Institute of Health, Bethesda, USA). The scale of image files obtained was 1.0 pixel = 4.2 μm, thus

allowing accurate measurements of the depth of microneedle penetration, the width of pore created, and the distance between the microneedle baseplate and the *stratum corneum*. All patches applied on the skin were carefully and gently removed from the skin after application. The applied skin sites were carefully examined using the microscope.

Mechanical fracture force of the microneedle patches was measured by Texture Analyzer set in compression mode. The microneedle patches were attached to the testing probe using adhesive tape and were driven against a flat block of aluminum at a rate of 0.05 mm/s until a force of 300 N was reached. The microneedle patches were observed by a microscope before and after the compression. The force and displacement data were used to quantitatively determine the fracture force.

2.5. Drug content analysis and drug delivery efficiency

The drug content of the patches was determined by completely dissolving the microneedle tips using the following solvents: acetonitrile for Nile red and DMSO for amphotericin B. The mixture was then centrifuged at 16,160 × g for 10 min and the supernatant was collected. The supernatant was then analyzed using reverse-phase High-Performance Liquid Chromatography (HPLC), as detailed in the analytical section below (Section 2.10).

The delivery efficiency of a patch was represented by the ratio of the amount of the drug delivered into the skin to the drug content in the patch. In order to quantify the amount of drug delivered into the skin, the skin was carefully cleaned with a wet paper towel after the removal of the patch. The skin was then cut into small pieces and soaked in the corresponding organic solvent (acetonitrile for Nile red and DMSO for amphotericin B). The mixtures were homogenized using a Tissue Lyser (Qiagen, Ltd., Manchester, UK) at 50 Hz for 20 mins. Centrifugation at 16,162 × g for 10 min was applied and the supernatant was collected. The supernatant was analyzed by HPLC.

2.6 Adhesion of dissolving base films and HFMB films to the neonate porcine skin

Dissolving base films were prepared by casting the dissolving base gel into MN0 moulds as described in Section 2.2.2. HFMB films were fabricated by casting HFMB gels into MN0 moulds and crosslinking the HFMB gels as described in Section 2.2.2. The adhesive properties of dissolving base films and HFMB films were assessed by a Texture Analyzer equipment using adhesive test mode. A piece of full thickness neonate porcine skin (around 1 mm thickness) was fixed into a poly(urethane) foam using pins and placed at the bottom of the measuring system and held in place by a clamp. Dissolving base films or HFMB films (1 cm^2) were soaked into PBS (pH 7.4) for 60 s and excess liquid on the film surface was gently

removed. These films were immediately affixed to the mobile probe using double-sided adhesive tape. The film was lowered at a speed of 0.50 mm/s to contact with the skin surface at a force of 5 N for a contact time of 10 s. It was then withdrawn at a speed of 0.50 mm/s to a distance of 50 mm. An acquisition rate of 200 points/s was set for the analysis. The adhesion of the films was evaluated in terms of peak detachment force and work of adhesion. The peak detachment force was recorded as the maximum force required to detach the film from the skin surface. The work of adhesion was also calculated from the area under the force-distance curve.

2.7 Disintegration and swelling properties of MN8 base in water

The hydrogel-forming microneedles base MN8 was studied in terms of its swelling and disintegration properties. The initial dry weight of MN8 was documented as m_0. The MN8 patches were then soaked in 40 mL of water for 24 h at room temperature. At predetermined time points, the patches were pictured, removed, dried with towel paper, and weighed as m_t. The swelling properties of the base microneedle patches MN8 were represented as the percentage of swelling, as shown in the following formula. The disintegration time was recorded based on the breakage of the patches.

$$\%\, Swelling = \frac{m_t - m_0}{m_0} \times 100\%$$

2.8 *In vitro* drug release study and biodegradation study

The amphotericin B PLGA C3 tips were cast in the moulds and collected. The amphotericin B PLGA C3 tips were then placed in 15 mL of release medium for the release study (n = 5). The release medium contained PBS and 1% w/v SLS. The experiment was conducted in the dark using a thermal incubator with 40 rpm and kept at 37 ± 1°C. Samples were taken at predetermined time points (1, 2, 3, 4, 5, 6, and 7 days) and the fresh release medium was added as appropriate. The samples were then quantified using HPLC after appropriate dilutions.

The cumulative drug released profile was fitted to various commonly-used mathematical kinetic models: zero-order, first-order, Higuchi and Korsmeyer-Peppas [27,28]. Only the portion corresponding to $\frac{Q_t}{Q_\infty} \leq 0.6$ was used to study the applicability of the models [28]. DDsolver (China Pharmaceutical University, Nanjing, China) was employed to calculate the model parameters [29]. The equations of mathematical kinetic models are presented as follows:

Zero-order: $Q_t = Q_0 + K_0 t$

First-order: $\ln Q_t = \ln Q_0 + K_1 t$

Higuchi: $Q_t = K_H \sqrt{t}$

Korsmeyer-Peppas: $\frac{Q_t}{Q_\infty} = K_{kP} t^n$

In these models, Q_t (%) is the percentage of drug released at time t, Q_0 is the initial value of Q_t, Q_∞ is the total amount of drug released, t is the time, n is the diffusion release exponent, K_0 , K_1, K_H and K_{KP} are the release coefficients corresponding to relevant kinetic models. The coefficient of determination (R^2) and Root of mean square error (RMSE) were used to evaluate the fit of a model equation.

The amphotericin B PLGA C3 tips were further investigated in their biodegradation. Amphotericin B-containing PLGA tips were collected and viewed using a Leica EZ4 D stereomicroscope (Leica Microsystems, Milton Keynes, UK) light microscope, where their lengths were measured. Afterwards they were placed in a 1.5 mL Eppendorf tube, where 1.5 mL of freshly prepared PBS solution (pH 7.4) was added. Samples were placed in 37°C shaking incubator at 40 rpm for 21 days to study their biodegradation. At predefined time points, PBS was withdrawn, the amphotericin B PLGA C3 tips were viewed *via* the light microscope, and measurements were taken. The difference in the length over time was recorded.

2.9 Disk diffusion test

Antifungal activity of the amphotericin B PLGA tipped C3-MN8 microneedle patches against *Candida albicans* NCYC 610 was determined using a modified radial diffusion assay [30]. Briefly, *Candida albicans* was cultivated overnight at 37ºC and 100 rpm in Sabouraud dextrose broth (SDB) before the experiment. The fungi were collected by centrifugation at 3000 rpm for 30 min and resuspended in fresh SDB. The optical density of the fungal suspension was set at 0.1 at 550 nm to obtain an equivalent to 6×10^6 CFU/mL. An aliquot of 1 mL of the fungal culture was then added to 5 mL of soft sabouraud dextrose agar and the mixture was then vortexed to ensure even distribution of the fungal cells. The mixture was then poured on the surface of the Sabouraud dextrose agar (SDA) plate. Finally, the amphotericin B PLGA-tipped microneedle patches C3-MN8, blank microneedle patches or a paper disc containing 400 µg of amphotericin B were placed in the centre of the plate and pressed gently with sterile forceps. The blank patch was fabricated by aligning PVP tips with MN8 without PLGA tips. All microneedle patches were applied for 30 s and removed immediately from the agar plates but

the paper disc stayed on the agar plates. After incubation at 37°C for 72 hours, the zone of inhibition around the patches was measured. The whole process was conducted under aseptic conditions and untreated inoculated plates were used as a control (n = 4).

2.10 Analytical methods for quantifying Nile red and amphotericin B

Quantification of Nile red and amphotericin B in all samples was carried out using HPLC Agilent Technologies 1220 Infinity Compact LC Series with Agilent degasser, binary pump, auto standard injector and UV detector (Agilent Technologies UK Ltd, Stockport, UK). The separation was achieved by using a C18 Phenomenex SphereClone™ analytical column (150 mm × 4.60 mm internal diameter, 5 µm packing). The instrumentation and chromatographic conditions for Nile red and amphotericin B are presented in Table 2. Agilent Chemostation® Software B.02.01 was used for the analysis of the chromatograms. These HPLC methods were validated according to the International Conference on Harmonization (ICH) guidelines for Validation of Analytical Procedures Q2 Analytical Validation Revision one (R1) 2005 [31].

Table 2. Parameters for HPLC analytical methods developed and validated for Nile red and amphotericin B.

Analyte	Mobile phase	Flow rate	Injection volume	UV	Column temperature
Nile red	water/acetonitrile, 20/80	1 mL/min	50 µL	550 nm	37ºC
Amphotericin B	Na_2EDTA (2.5 mM) /methanol/acetonitrile/tetrahydrofuran, 35/39/17/9	1 mL/min	50 µL	385 nm	30ºC

2.11 Statistical analysis

All quantitative data were expressed as means ± standard deviation (SD) from triplicate measurements unless otherwise noted. Differences between groups were assessed for significance using one-way analysis of variance (ANOVA), followed by a multiple comparisons test (Tukey's test). The threshold for significance was $p< 0.05$. Statistical analysis was performed using Prism 7 (GraphPad Software, San Diego, CA, USA).

3. Results

3.1 Fabrication of Nile red PLGA-tipped dissolving base microneedle patches

Nile red PLGA-tipped dissolving base microneedle patches were fabricated by casting Nile red PLGA tips multiple times and then casting dissolving pedestals which were subsequently attached to the dissolving baseplate (MN0). The needles of the microneedle patches consisted of two parts, Nile red PLGA tips and dissolving pedestals cast from PVP. The digital microscope images (Figure 2A, 2B) show that Nile red was specifically entrapped at the tip of the needles. Moreover, the scanning electron microscope (SEM) image of C2-MN0 (Figure 2C) reveals a clear dividing line between the tips and the pedestals. Those observations indicate the successful manufacture of a two-layer microneedle system with the implanted elements only found in the tips and dissolving pedestals proximal to the dissolving baseplate (MN0).

A range of replicates of Nile red PLGA solution casting procedures were then performed. As presented in Figures 2B and 2D, the portion of the implantable Nile red PLGA tips increased in length with the increase of casting replicates. Accordingly, the dissolving pedestal portion gradually decreased with the increase of casting replicates. The length of the Nile red PLGA tip was 301 ± 14 μm for C1-MN0, 404 ± 3 μm for C2-MN0, 482 ± 13 μm for C3-MN0, and 529 ± 1 μm for C4-MN0. The proportion of Nile red PLGA tips of C1-MN0, C2-MN0, C3-MN0, and C4-MN0 to the total needle length (i.e. 600 μm) increased from 50.2% ± 2.3% to 88.2% ± 0.2%. This indicated the implantable portion of the tips could be customized through a simple variation of the solution casting process.

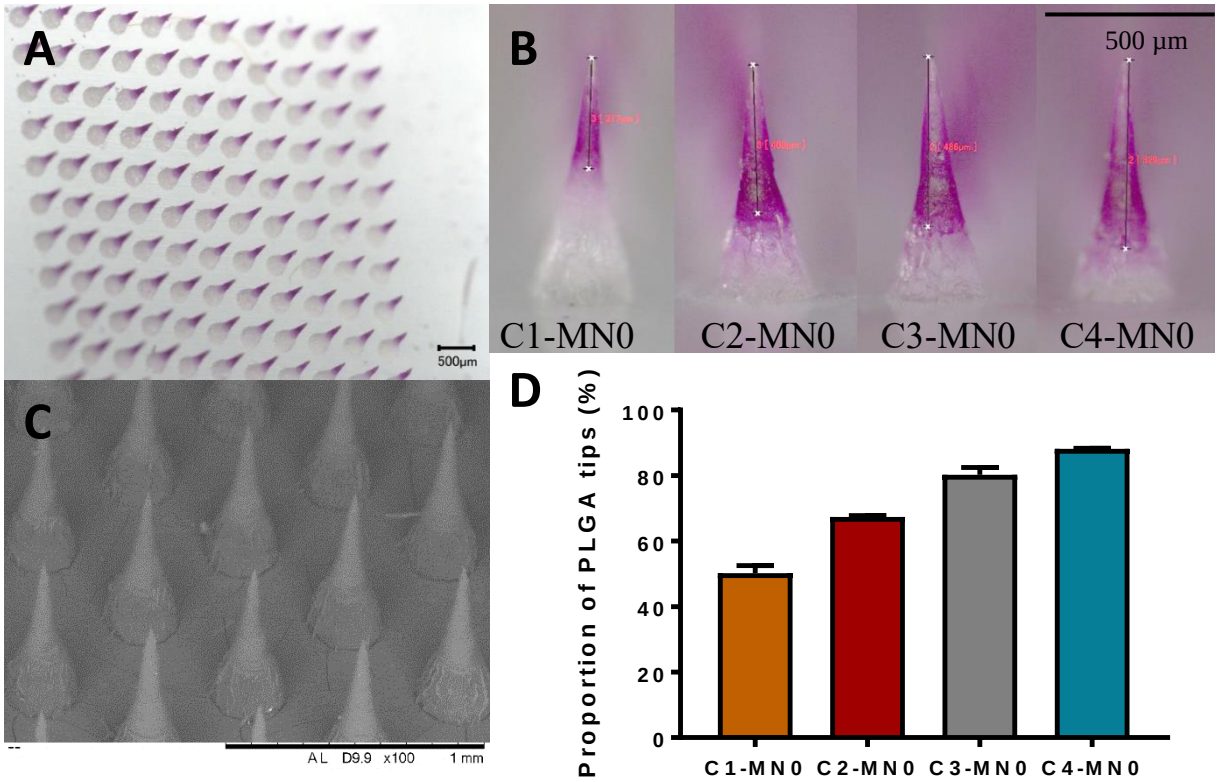

Figure 2. Characterization of Nile red PLGA-tipped microneedle patches fabricated with varying numbers of casting procedures. (A) A microscopy image of C2-MN0. Scale bar, 500 µm. (B) Representative images of a single tip in C1-MN0, C2-MN0, C3-MN0, and C4-MN0 PLGA-tipped microneedle patches. Scale bar, 500 µm. (C) A scanning electron microscope image of C2-MN0. Scale bar, 1 mm. (D) The proportion of PLGA tips to needles in length for C1-MN0, C2-MN0, C3-MN0, and C4-MN0. (Means + S.D., n = 3).

3.2. Drug content analysis of Nile red PLGA-tipped dissolving base microneedle patches

The drug content of C1-MN0, C2-MN0, C3-MN0, and C4-MN0 was 0.55 ± 0.11 µg, 0.97 ± 0.05 µg, 2.05 ± 0.23 µg and 2.67 ± 0.30 µg, respectively (Figure 3D). Thus, it can be concluded that the drug content increased with the increase of casting replicates. If the content of Nile red in a patch was assumed to be directly proportional to the concentration of Nile red in the casting solution, the maximum amount of Nile red one patch could carry would be limited by the solubility of Nile red in a certain solvent. Thus, the solubility of Nile red in different solvents was measured using HPLC. The estimated maximum drug content that one patch could carry using a certain kind of solvent to prepare the casting solution was also calculated. As presented in Table 3, the best solvent among the five tested for Nile red was chloroform. With a saturated solution of Nile red in chloroform, the patch could carry around 100 µg of Nile red.

Table 3. The solubility of Nile red in different solvents and estimated maximum drug content if cast by the saturated solution of the solvent.

Solvents	Solubility (mg/mL)	Estimated maximum drug content per patch (µg)
Acetonitrile	1.46 ± 0.03	7.47
Acetone	2.04 ± 0.00	10.44
Tetrahydrofuran	11.40 ± 0.00	58.33
TFE	6.71 ± 0.00	34.33
Chloroform	20.75 ± 0.03	106.17

3.3. *In vitro* mechanical performance of Nile red PLGA-tipped dissolving base microneedle patches

A successful microneedle delivery system should possess sufficient mechanical properties for reliable skin penetration to achieve efficient drug delivery. Herein, the insertion performance of C1-MN0, C2-MN0, C3-MN0, and C4-MN0 was examined *in vitro* using standard commercial Parafilm M® as a previously validated skin simulant [22]. Figure 3A shows that all microneedle patches were able to penetrate the first layer of Parafilm M® and reached a depth of at least 126 µm. However, for the second layer, the mean values of holes created in the second layer of Parafilm M® decreased with the increase of casting replicates (Figure 3B). C4-MN0 exhibited the worst penetration ability with 20.9% ± 8.1% penetration into the second layer. These data were significantly different compared with those of C1-MN0 (69.4% ± 29.4%) or C2-MN0 (45.0% ± 13.8%) ($p < 0.05$). This indicated that the increase in the length of PLGA Nile red tip (i.e. PLGA and Nile red) or the decrease of the length of the dissolving pedestals (PVP) possibly had a tendency to weaken the insertion depth of the microneedle patches. Figure 3C shows that there was no significant difference for different microneedle patches in height reduction after compression at 32 N for 30 s ($p > 0.05$). The force of 32 N was chosen as it was shown to be the mean force exerted by human volunteers applying microneedle patches into their skin [22,32]. All microneedle patches withstood the 32 N force with less than 20% height reduction, indicating the microneedle tips were not fragile.

A force starting from 0 N up to 300 N was applied to C1-MN0, C2-MN0, C3-MN0, and C4-MN0 to determine the patches' failure force. The microneedle tips failed in a bent shape rather than fracture under such a force. The microneedle tips after compression are presented in Figure 3F (C1-MN0), Figure 3G (C2-MN0), Figure 3H (C3-MN0) and Figure 3I (C4-MN0). Those data also indicated that the microneedles of Nile red PLGA-tipped dissolving base microneedle patches were rather soft than fragile. This test was developed by applying pressure against an aluminum surface, which is not representative of the real insertion scenario. The baseplate of some patches was fractured as observed an abrupt decrease in

the force (as pointed by the arrow in Figure 3E). The fracture force of the baseplate was in the range of 70 N to 260 N, which is higher than the average maximum human manual force as reported in the literature [22].

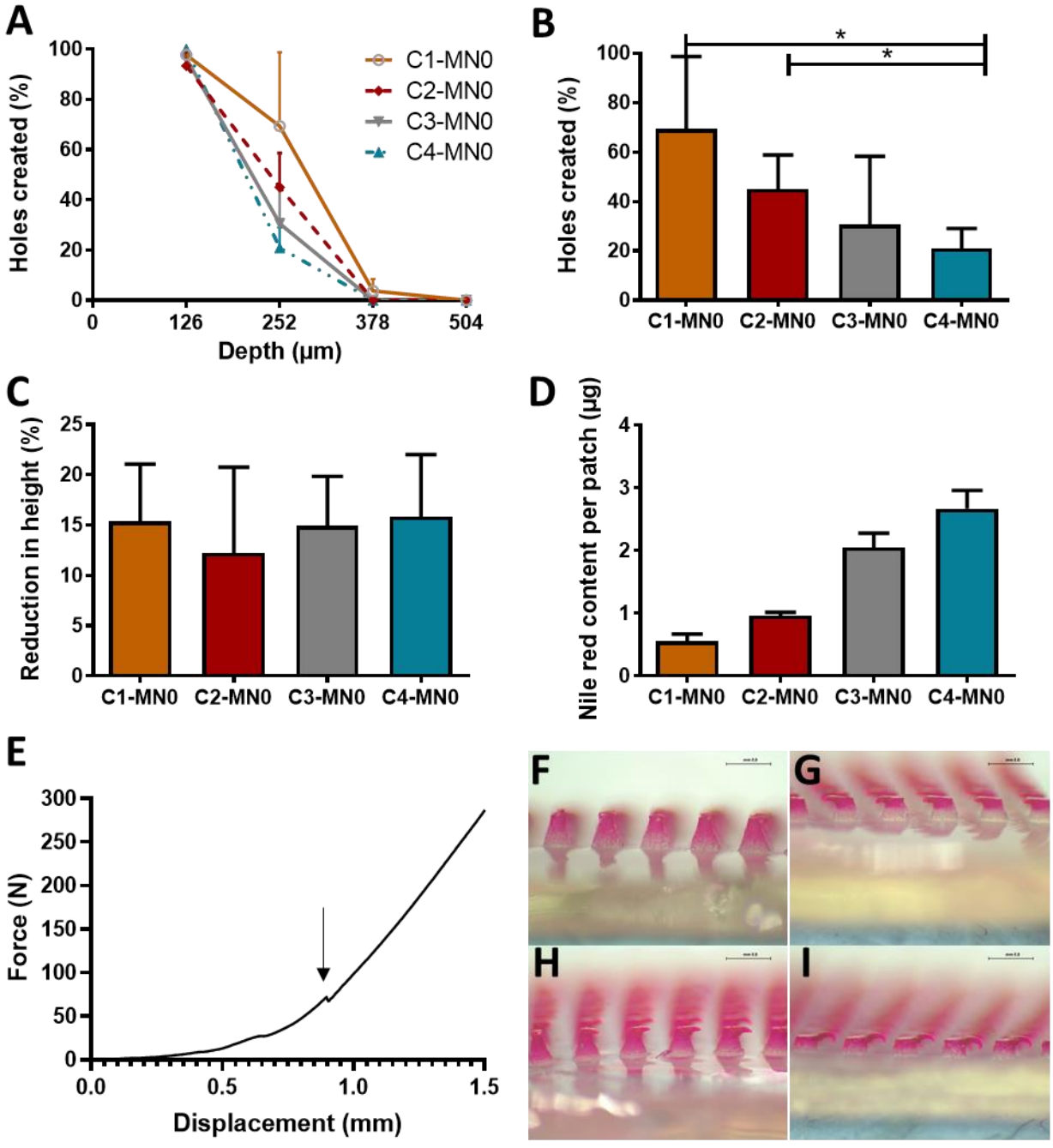

Figure 3. *In vitro* insertion performance of Nile red PLGA-tipped microneedle patches. (A) Percentage of holes created in each Parafilm M® layer following insertion of C1-MN0, C2-MN0, C3-MN0 and C4-MN0 using a force of 32 N/array. (B) Percentage of holes created in the second layer of Parafilm M®. (C) Percentage of height reduction of needles in microneedle patches after compression at 32 N/array. (D) The drug content of Nile red in C1-MN0, C2-MN0, C3-MN0, and C4-MN0. (Means + S.D., n = 3) (* $p < 0.05$). (E) Representative plot of fracture force determination of Nile red PLGA-tipped microneedle patches. (F) C1-MN0, (G) C2-MN0, (H) C3-MN0, and (I) C4-MN0 microneedle patches after a 300 N's compression.

3.4 Optimisation of the base design in the Nile red PLGA-tipped microneedle patches

An ex vivo skin insertion test (Figure S1 in Supplementary information) showed incomplete implantation of C4-MN0 tips in the porcine skin, indicating the insertion depth of the C4-MN0 was not sufficient to implant the Nile red PLGA C4 tips inside the skin. Accordingly, two adjustments were made to improve the implantation. Firstly, the length of the PLGA tips was reduced from 529 µm ± 1 µm (C4) to 404 µm ± 3 µm (C2). Secondly, the HFMB MN6 and MN8 were aligned with the PLGA tips to increase the insertion depth. Therefore, C2-MN6 and C2-MN8, as well as C2-MN0, were fabricated and are presented in Figure 4. The length of the whole needle in C2-MN0 was 634 µm ± 17 µm, in C2-MN6 was 686 µm ± 45 µm and in C2-MN8 was 970 µm ± 8 µm (n = 3).

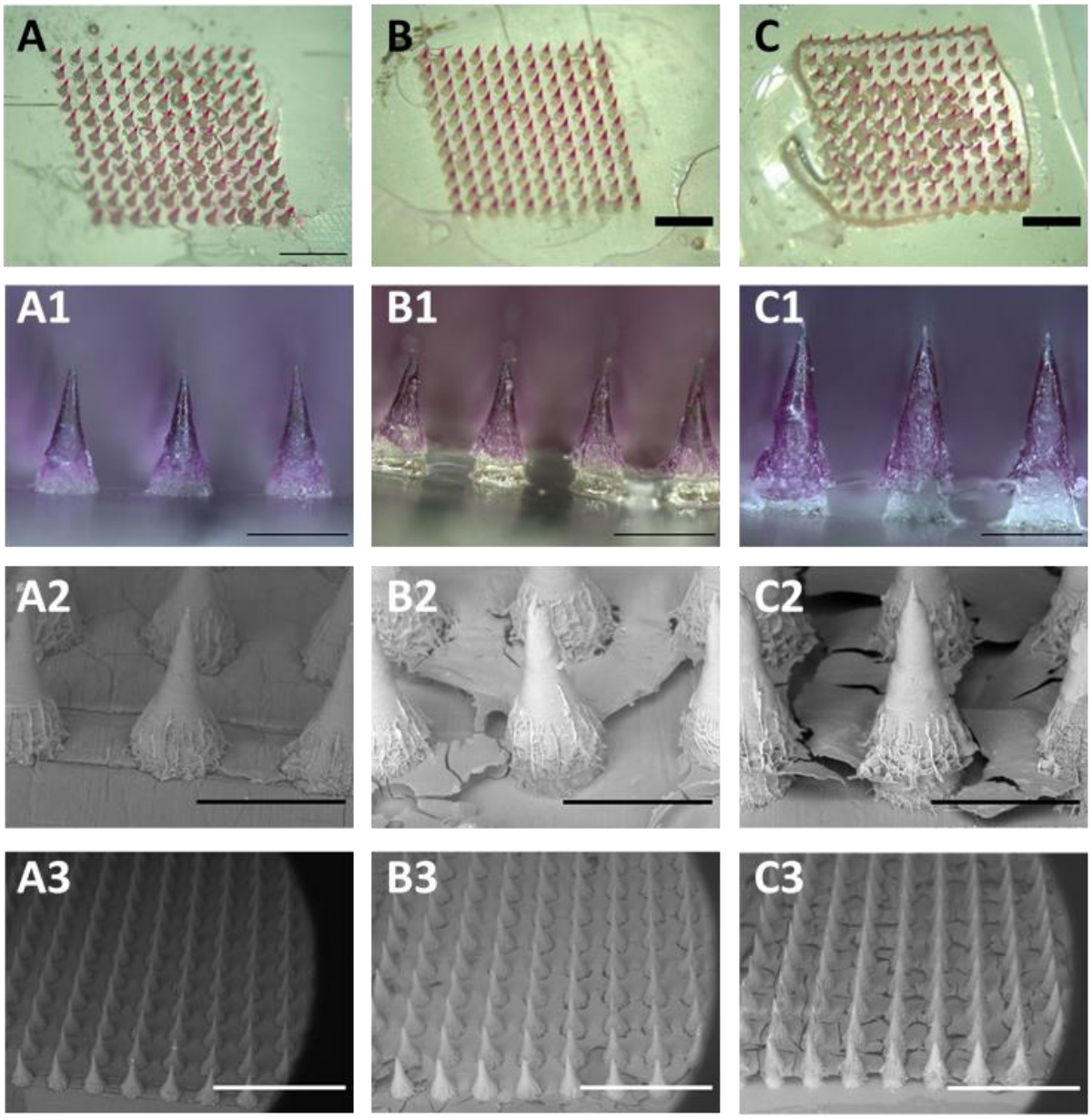

Figure 4. Nile red PLGA-tipped microneedle patches. Microscopic pictures of (A) C2-MN0, (B) C2-MN6, and (C) C2-MN8. Scale bar, 2 mm. Microscopic pictures of tips in (A1) C2-MN0, (B1) C2-MN6, and (C1) C2-MN8. Scale bar, 500 µm. SEM pictures of tips in (A2) C2-MN0, (B2) C2-MN6, and (C2) C2-MN8. Scale bar, 500 µm. SEM pictures of (A3) C2-MN0, (B3) C2-MN6, and (C3) C2-MN8. Scale bar, 2 mm.

3.5 *In vitro* insertion performance of the optimised Nile red PLGA-tipped microneedle patches

Parafilm M® was used to evaluate the effect of the base designs on the insertion properties of the PLGA-tipped microneedle patches, as previously performed for C1-C4 MN0 patches. The holes created in the Parafilm M® layers were counted as an index of insertion depth (as provided in Figure S2 in Supplementary information). As shown in Figure 5A, C2-MN0 was able to penetrate the second layer, while C2-MN6 and C2-MN8 were able to penetrate the

fourth layer. C2-MN0 was inserted up to 252 µm, while C2-MN6 and C2-MN were inserted up to 504 µm. These results were corroborated by OCT (Figures 5C-E). In the fourth layer of the Parafilm M®, C2-MN0 created 0% of holes, C2-MN6 created 33.88% ± 4.37% holes, and C2-MN8 created 93.66% ± 5.38% holes (Figure 5B). There was a significant difference between C2-MN0 and C2-MN6 ($p < 0.001$), C2-MN0 and C2-MN8 ($p < 0.0001$), C2-MN6 and C2-MN8 ($p < 0.0001$). The insertion profiles of these three types of microneedle patches cannot be directly compared due to their different needle lengths. However, this test was designed to evaluate if the insertion depths were sufficient to guarantee PLGA tip implantation within the skin.

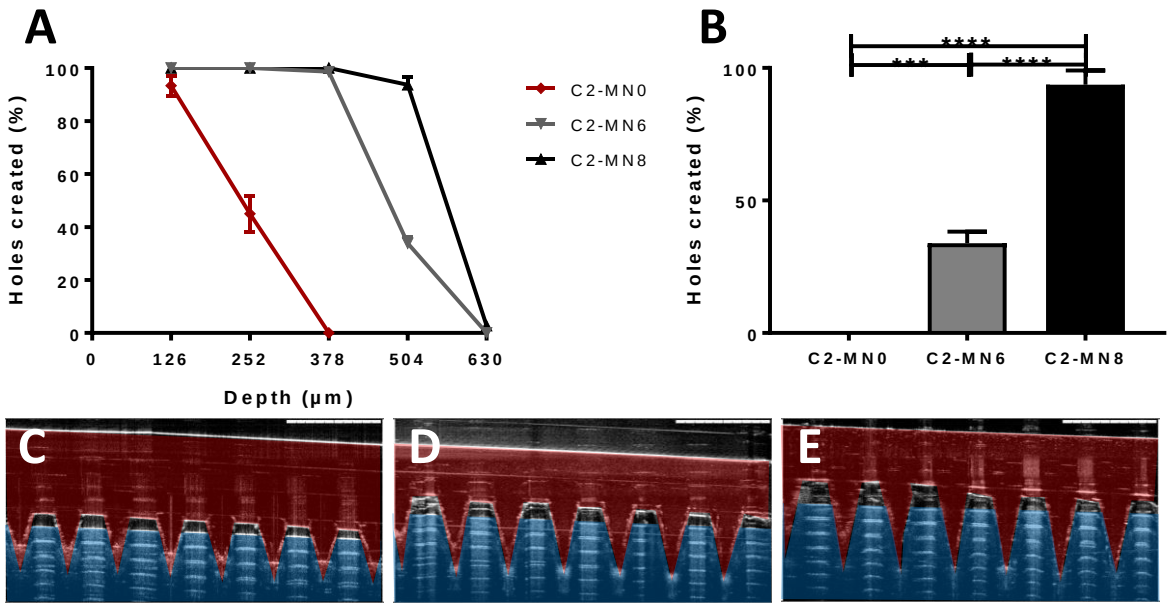

Figure 5. *In vitro* insertion into Parafilm M® of Nile red PLGA-tipped microneedle patches. (A) Percentage of holes created in each Parafilm M® layer following insertion of Nile red PLGA-tipped microneedle patches. (B) Percentage of holes created in the third layer of Parafilm M®. (Means ± S.D., n = 4) (***$p < 0.001$, ****$p < 0.0001$). Representative OCT picture immediately after insertion into Parafilm M® layers of (C) C2-MN0, (D) C2-MN6, and (E) C2-MN8. Scale bar = 1 mm.

3.6 *Ex vivo* skin insertion performances and delivery efficiency of the optimised Nile red PLGA-tipped microneedle patches

Ex vivo porcine skin insertion tests were used to evaluate the delivery efficiency of C2-MN0, C2-MN6 and C2-MN8. The application time for C2-MN6 and C2-MN8 was 30 s while that for C2-MN0 was 3 min and kept in skin for 30 min in total to make sure the dissolving pedestals in C2-MN0 had time to fully dissolve. The drug delivery efficiency was represented as the ratio of the drug deposited inside the skin to the drug carried in the patch. As can be observed in

Figures 6A (C2-MN0), 6B (C2-MN6) and 6C (C2-MN8), all the needles were sharp and the Nile red was uniformly distributed in the tips. Moreover, a clear dividing line between dissolving pedestals and the HFMB MN6 or MN8 was observed in C2-MN6 (Figure 6B) and C2-MN8 (Figure 6C).

Since Nile red has a red colour, skin insertion pictures were able to visualize the inserted drug-containing tips. Figure 6A1 shows that C2-MN0 was able to indent the skin, but only deposited a very limited number of tips in the skin. C2-MN6 inserted almost all the tips, as can be observed in Figure 6B1. However, some tips in C2-MN6 were not totally beneath the skin surface, as the pictures showed some tips were lying on the skin surface. C2-MN8 was able to insert almost all the tips and, more importantly, the tips were fully embedded in the skin beneath the skin surface so that only the end of the tips was seen (Figure 6C1).

OCT was used to vertically scan the skin in situ, thus allowing the visualizing of the tips inside the skin in real time. As presented in Figure 6A2, the tips of C2-MN0 were only partially inserted in the skin and some of the tips were lying above the skin surface. Figure 6B2 shows that the tips of C2-MN6 were partially inside the skin. By contrast, the tips of C2-MN8 were fully embedded beneath the skin surface as noticed by the closure of the skin surface, which is displayed in Figure 6C2.

Figure 6D shows the drug delivery efficiency of C2-MN0, C2-MN6 and C2-MN8. C2-MN0 deposited 39.35% ± 10.01% of the drug from the patch inside the skin, C2-MN6 deposited 55.83% ± 19.61%, while C2-MN8 deposited 83.72% ± 20.63% of the Nile red from the patch in the skin. The mean value of the drug deposited increased as the increase of the needle lengths of the HFMB that were aligned with the tips. A significant difference was noticed between C2-MN0 and C2-MN8 ($*p < 0.05$).

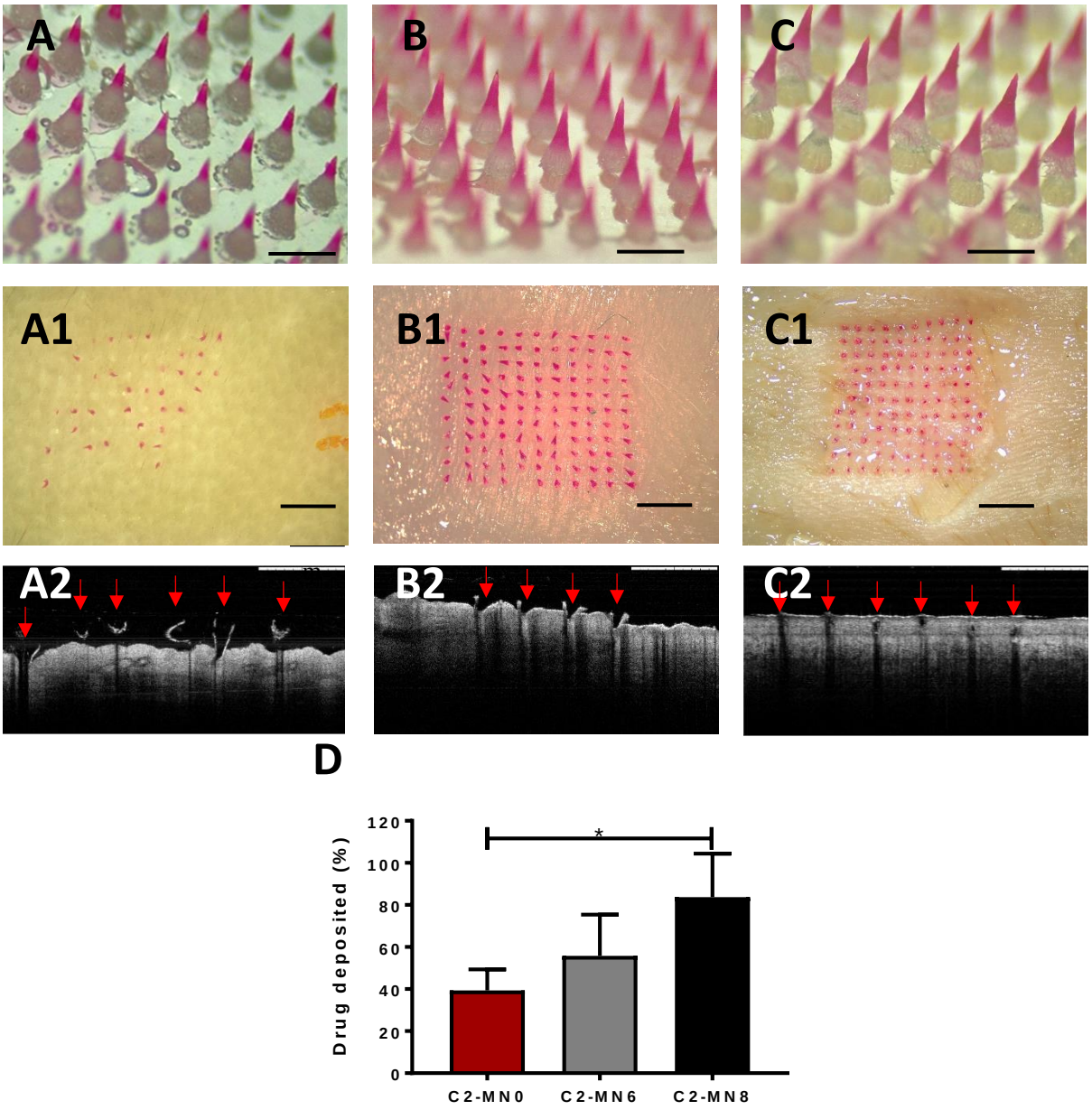

Figure 6. Detailed pictures of Nile red PLGA-tipped microneedle patches before insertion (A) C2-MN0, (B) C2-MN6, and (C) C2-MN8. Scale bar, 1 mm. Images of the skin after insertion of (A1) C2-MN0, (B1) C2-MN6, and (C1) C2-MN8. Scale bar, 2 mm. OCT images of the insertion process of (A2) C2-MN0, (B2) C2-MN6, and (C2) C2-MN8. The PLGA tips were indicated by the arrows Scale bar, 1 mm. (D) Percentage of the drug from the patch deposited in the skin (Means + S.D., n = 4). (*p< 0.05)

3.7 Fabrication and *in vitro* insertion performance of amphotericin B PLGA-tipped microneedle patches

Amphotericin B PLGA-tipped microneedle patches were produced using the same procedure as Nile red PLGA-tipped microneedle patches, as can be observed in Figure 7A for C3-MN6. An *in vitro* insertion examination was performed to investigate the effect of the increased

casting replicates of amphotericin B PLGA tips on the insertion ability of the microneedle systems. Multiple casting procedures were performed to form C1-MN6 (casting once), C2-MN6 (casting twice) and C3-MN6 (casting three times). *In vitro* insertion into Parafilm M® was performed by using a force of 32 N to insert these amphotericin B PLGA-tipped microneedle patches into Parafilm M® layers. The holes created in the Parafilm M® layers were counted as an indication of the insertion depth (as provided in Figure S3 in Supplementary information). As shown in Figure 7B, C1-MN6 was able to penetrate the third layer, while C2-MN6 and C3-MN6 were able to penetrate the fourth layer. In the third layer of Parafilm M® layers, as shown in Figure 7C, C1-MN6 created 36.98% ± 4.83% of holes, C2-MN6 created 65.29% ± 16.69% holes, and C3-MN6 created 93.39% ± 5.96% holes. There was a significant difference between C1-MN6 and C2-MN6 ($p < 0.05$), C2-MN6 and C3-MN6 ($p < 0.05$), C1-MN6 and C3-MN6 ($p < 0.001$). OCT images in Figure 7D, E, F represent the insertion behaviour of C1-MN6, C2-MN6, and C3-MN6, respectively. The needles of C1-MN6 (Figure 7D) penetrated between the second and the third layer of the Parafilm M® layers, the needles of C2-MN6 (Figure 7E) fell between the third and the fourth layer of the Parafilm M® layers, and the needles of C3-MN8 (Figure 7F) reached between the third and the fourth layer of the Parafilm M® layers. As suggested by the OCT and Parafilm M® layers, the insertion depth for C1-MN6 was about 252 – 378 µm, that for C2-MN6 was 378 – 504 µm, and that for C3-MN6 was 378 – 504 µm.

3.8 Drug content analysis of amphotericin B PLGA-tipped microneedle patches

The drug content was analyzed for C1-MN6, C2-MN6, and C3-MN6. As presented in Figure 7G, the drug content of C1-MN6, C2-MN6, and C3-MN6 was 66.11 ± 3.34 µg, 89.16 ± 7.89 µg, and 160.00 ± 7.36 µg, respectively. It can be concluded that the drug content increased with the increase of casting replicates. It was noticed that there was a significant difference between C1-MN6 and C2-MN6 (**$p < 0.01$), between C2-MN6 and C3-MN6 (****$p < 0.0001$), and between C1-MN6 and C3-MN6 (****$p < 0.0001$).

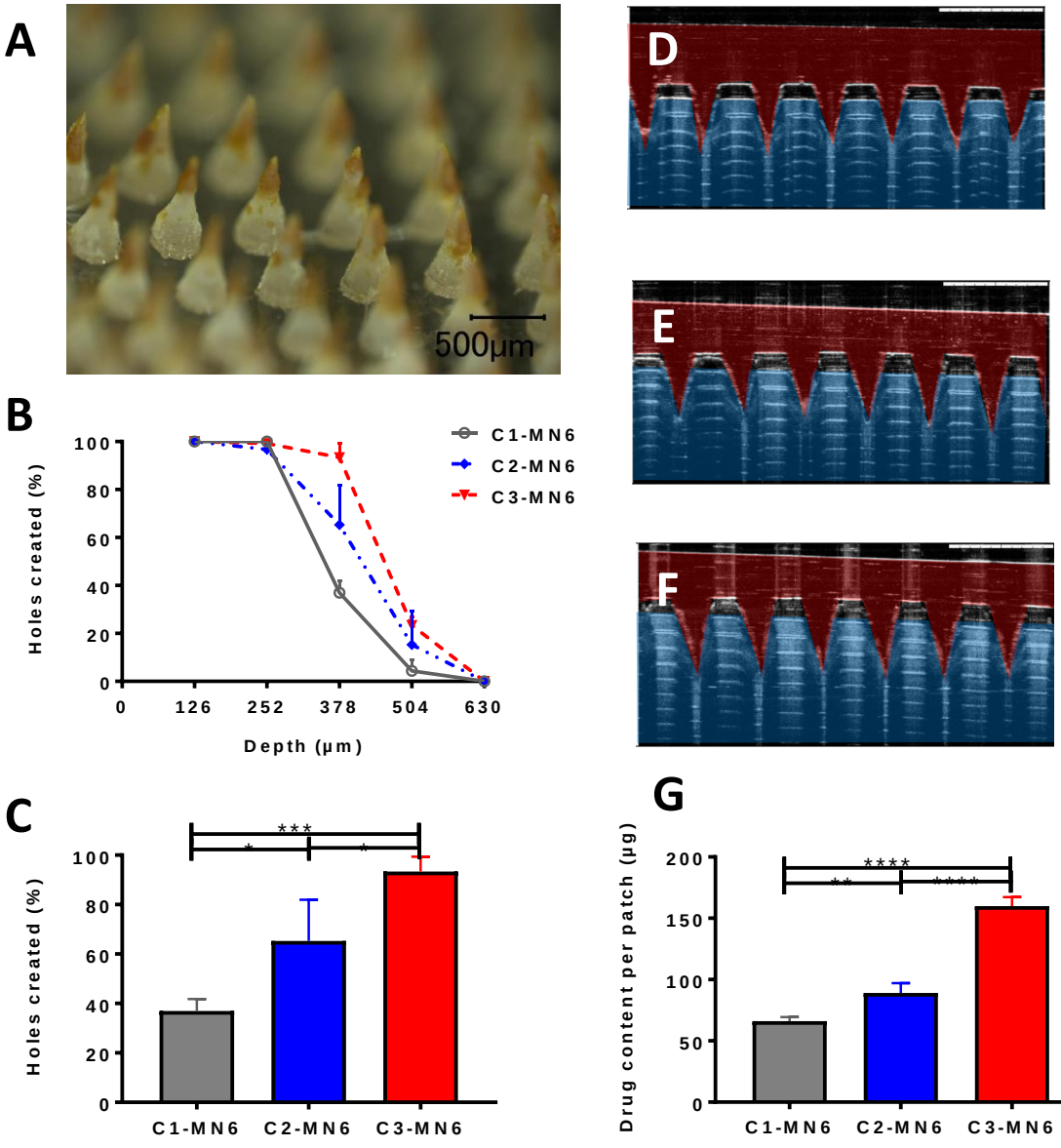

Figure 7. Fabrication and *in vitro* insertion into Parafilm M® of amphotericin B PLGA-tipped microneedle patches. (A) A representative picture of C3-MN6. Scale bar = 500 µm. (B) Percentage of holes created in each Parafilm M® layer following insertion. (Means + S.D., n = 3). (C) Percentage of holes created in the third layer of Parafilm M®. (Means + S.D., n = 3). Representative OCT picture immediately after insertion into Parafilm M® layers of (D) C1-MN6, (E) C2-MN6, and (F) C3-MN6. Scale bar = 1 mm. (G) Amphotericin B content in amphotericin B PLGA-tipped microneedle patches C1-MN6, C2-MN6, and C3-MN6 (Means + S.D., n = 3) (*$p < 0.05$, **$p < 0.01$, ***$p < 0.001$, ****$p < 0.0001$).

3.9 Optimisation of the base design in the amphotericin B PLGA-tipped microneedle patches

As amphotericin B PLGA C3 tips contained the highest amount of drug (160.00 ± 7.36 µg) and achieved the highest insertion percentage *in vitro* insertion percentage, amphotericin B PLGA

C3 tips were chosen to align with different base designs to produce amphotericin B PLGA-tipped microneedle patches C3-MN0, C3-MN6, and C3-MN8. The digital microscope and SEM images were presented to visualize the patches and the difference in the structure of the microneedle tips (Figure 8). Amphotericin B was only present in the tips of the patches, which was very clear due to the yellow colour of the compound. There was an obvious dividing line of the needles in C3-MN8, as the tips were fabricated using a mould with a depth of 600 µm and MN8 were fabricated using a mould with a depth of 800 µm.

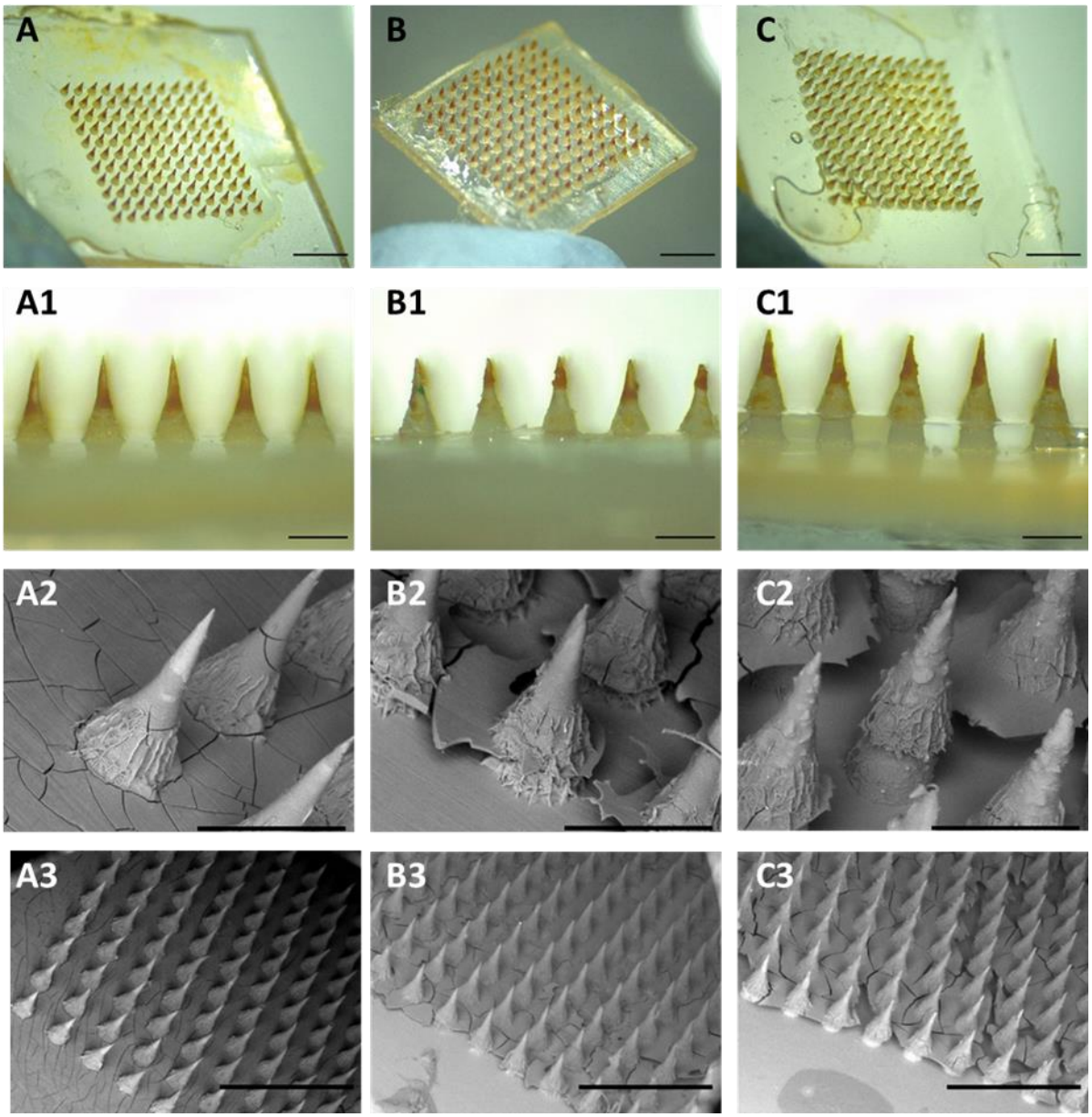

Figure 8. Amphotericin B PLGA-tipped microneedle patches. Microscopic pictures of (A) C3-MN0, (B) C3-MN6, and (C) C3-MN8. Scale bar, 2 mm. Microscopic pictures of tips in (A1) C3-MN0, (B1) C3-MN6, and (C1) C3-MN8. Scale bar, 500 µm. Scanning electron microscope pictures of tips in (A2) C3-MN0, (B2) C3-MN6, and (C2) C3-MN8. Scale bar, 500 µm. Scanning electron microscope pictures of (A3) C3-MN0, (B3) C3-MN6, and (C3) C3-MN8. Scale bar, 2 mm.

3.10 *Ex vivo* skin insertion behaviour and delivery efficiency of the optimised amphotericin B PLGA-tipped microneedle patches

Ex vivo porcine skin insertion tests were performed to test the delivery efficiency of the C3-patches with different base designs, i.e. C3-MN0, C3-MN6 and C3-MN8, to further investigate delivery efficiency using different base designs.

From the detailed pictures of C3-MN0, C3-MN6 and C3-MN8 (Figures 9A-C), it was noticed that all the needles were sharp and the amphotericin B was distributed evenly in the tips. Amphotericin B is a bright yellow compound. Therefore, the amphotericin B deposited in the skin was easy to identify. C3-MN0 only deposited a limited number of tips in the skin, as observed in Figure 9A1. C3-MN6 inserted most of the tips inside the skin, as presented in Figure 9B1. C3-MN8 inserted almost all the tips and what is probably more important, the tips were embedded in the skin so just the end of the tips were seen (Figure 9C1).

The delivery efficiency of C3-MN0, C3-MN6 and C3-MN8 is presented in Figure 9D. C3-MN0 deposited 21.63% ± 9.52% (33.75 ± 14.85 µg) of the drug inside the skin, C3-MN6 deposited 53.70% ± 17.46% (83.76 ± 27.24 µg), while C3-MN8 deposited 86.99% ± 11.62% (130.48 ± 17.43 µg) of amphotericin B from the patch inside the skin. The amount of the deposited drug increased with the increase of the lengths of needles of HFMB aligned with the tips. A significant difference was found between C3-MN0 and C3-MN6 (*$p < 0.05$), C3-MN6 and C3-MN8 (*$p < 0.05$), and between C3-MN0 and C3-MN8 (****$p < 0.0001$).

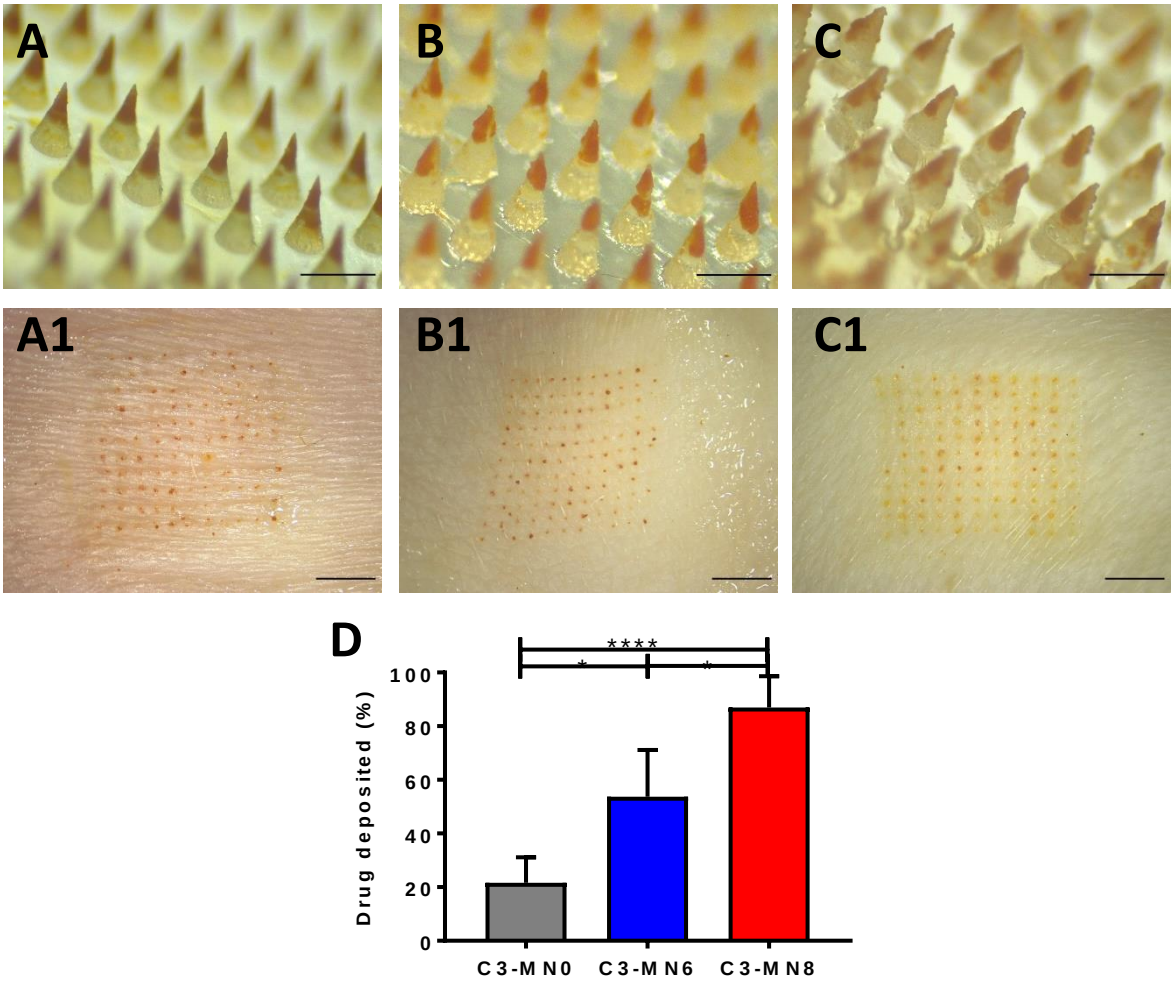

Figure 9. Amphotericin B PLGA-tipped microneedle patches (A) C3-MN0, (B) C3-MN6, and (C) C3-MN8. Scale bar, 1 mm. Skin deposition of (A1) C3-MN0, (B1) C3-MN6, and (C1) C3-MN8. Scale bar, 2 mm. (D) The percentage of the drug deposited in the skin to the drug in a patch. (Means + S.D., n = 4) (**p < 0.01, ****p < 0.0001).

3.11 Adhesion of dissolving base film and hydrogel base film to neonate porcine skin

Adhesion properties measured in this study was to check the ease of peeling the bases off from the skin surface after microneedle application. Generally, the adhesion of films increases with the degree of hydration until a point where overhydration leads to an abrupt drop in adhesive strength due to disentanglement at the polymer/tissue interface. The films were therefore soaked in PBS (pH 7.4) for 60 s to allow the polymer chains to fully hydrate prior to testing and excess water was removed before test. As shown in Figure 10A, the peak detachment force for the dissolving base films was 1.089 ± 0.1817 N. HFMB films presented a significantly lower peak detachment force at 0.3748 ± 0.1133 N (p < 0.01). As shown in Figure 10B, the work of adhesion of HFMB films was 0.0595 ± 0.0663 mJ, which was much lower than that of dissolving film (5.641 ± 1.057 mJ, p < 0.001). Those results indicated that

HFMB films were easier to peel off from the skin than the dissolving base film in terms of the peak detachment force or work needed to remove them.

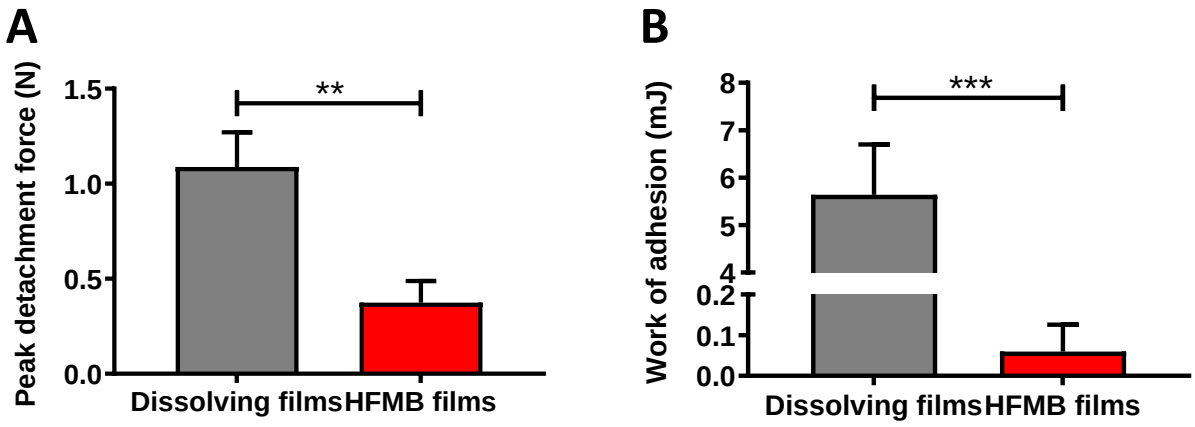

Figure 10. Adhesion properties of dissolving films and HFMB films. (A) The peak detachment force for dissolving films and HFMB films. (B) The work needed to detach the dissolving films and HFMB films from the porcine skin. (**$p < 0.01$, ***$p < 0.001$).

3.12 Swelling and disintegration properties of MN8 base in water

The swelling properties of MN8 was investigated to understand the interaction between MN8 and water. As displayed in Figure 11A, MN8 absorbed water gradually and the swelling percentage at equilibrium for 24 h was 106.20% ± 19.39%. As the weight was constantly increased after MN8 immersed in water, the swelling of MN8 was dominant instead of dissolving behavior. Figure 11B shows the MN8 before being immersed in water. At 15 min (Figure 11C), it started to break. However, the size of MN8 did not change significantly. At 30 min (Figure 11D), MN8 swelled and broke into smaller pieces. After implanting the tips of C3-MN8 patches into the skin, MN8 would be left and might generate biohazard waste. The disintegration study indicated an easy way to disable MN8 by immersing it into water for over 15 min.

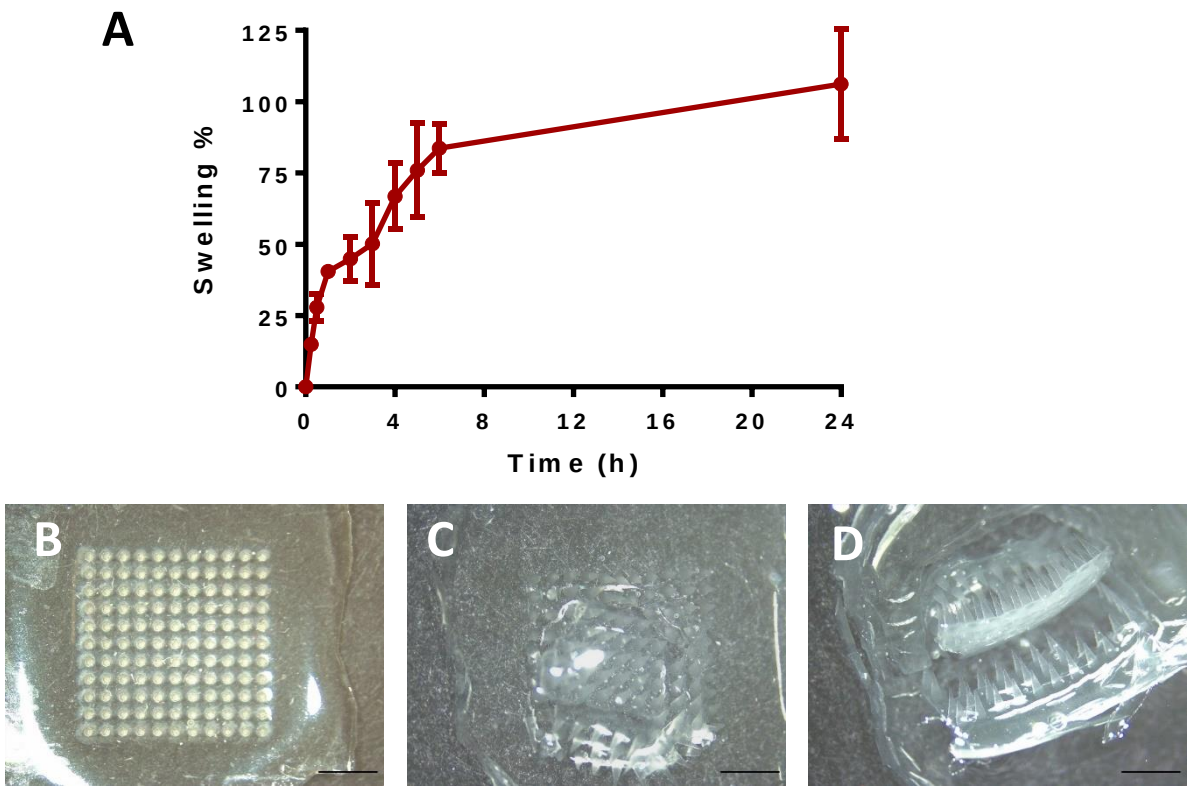

Figure 11. The swelling and disintegration properties of MN8 base in water. (A) Swelling percentage of MN8 in water. (Means ± SD, n = 4). Representative images of MN8 soaked in water at different time points (B) 0 min, (C) 15 min, (D) 30 min. Scale bar, 2 mm.

3.13 *In vitro* release study and biodegradation study

The in vitro release profile of amphotericin B from PLGA C3 tips is shown in Figure 12A. The release profile shows that amphotericin B was released from the C3 tips for seven days in the release medium (PBS, pH 7.4, containing 1% w/v SLS). On the first three days, the release was relatively constant over time and 72.42% ± 7.34% of the drug was released into the medium.

The release mechanism of the amphotericin B PLGA C3 tips and the kinetic order of drug release from the tips were studied by fitting the *in vitro* drug release data into different kinetic models, which included the zero-order, first-order, Higuchi, and Korsmeyer-Peppas. Table 4 shows the results of the correlation coefficient of each model. It is worth noting that the n value for Korsmeyer-Peppas modelling is 1.076, which is greater than 0.89. Accordingly, the release mechanism of the drug from PLGA tips was super case-II transport. This indicated that the rate of solvent diffusion was the determining factor of the diffusion [33]. The zero-order model fits well with the release profile (R^2 = 0.9964). The zero-order model reveals the process of

constant drug release from a drug delivery device independent of the concentration, which is ideal for a dosage form and leads to minimum fluctuations in drug plasma levels [34].

Table 4. Mathematical models of the kinetics release of amphotericin B from PLGA tips.

Mathematical model	Zero-order	First-order	Higuchi	Korsmeyer-Peppas
R^2	0.9964	0.9572	0.8908	0.9979
RMSE	1.9024	6.5674	10.4903	1.7968

With regard to the biodegradation of amphotericin B PLGA C3 tips, it was observed that the number and the length of tips was decreasing over 21 days (as shown in Figure S4 in Supplementary information). This demonstrated that the C3 tips were biodegrading over time. To further confirm those findings, the tips lengths were recorded, where the reduction in size was depicted in Figure 12B. It shows that the length of the C3 tips was reduced by more than 50% of its original length over 3 weeks.

3.14 Disk diffusion test

C3-MN8 microneedle patches showed the highest rate of amphotericin B delivery efficiency. Therefore, these patches and PVP-tipped MN8 microneedle patch groups were used to perform a modified disk diffusion test against the growth of *Candida albicans* (Figure 12C). The amphotericin B PLGA-tipped C3-MN8 microneedle patches or blank microneedle patches were inserted in the agar plate for 30 s and removed immediately as performed in the skin insertion study. These microneedle patches were applied on the agar plate for 30 s to check if the PLGA drug containing tips could be deposited in the agar plate in such a short application time, if the inserted microneedle tips could release the drug, and if the drug was still effective to inhibit the growth of the fungal. The blank microneedle patches, which were made of PVP aligned with MN8 without amphotericin B PLGA tips, showed no zone of inhibition, indicating PVP and MN8 had no inhibitory effect on fungal growth. As evidenced in Figure 12E, *Candida albicans* occupied the site of the blank microneedle indentation in the agar plate. The tips of C3-MN8 were clearly able to be deposited in the agar plate within an application time of 30 s (Figure 12D). The amphotericin B PLGA-tipped C3-MN8 microneedle group showed remarkable inhibition of *Candida albicans* with a zone area of 284.9 ± 20.6 mm^2, which equals to a circle with a radius of 9.5 ± 0.5 mm. The paper disc with 400 µg of amphotericin B was placed on top of the agar during the incubation and formed an inhibition zone of an area of 143.3 ± 12.2 mm^2 with a radium of 6.8 ± 0.3 mm (Figure 12F), which is smaller than that of amphotericin B PLGA tips. This suggested that the PLGA tips could release amphotericin B into the agar plate in a wider area than the paper disc. These results indicated that

amphotericin B PLGA-tipped C3-MN8 microneedle patches deposited drug-containing tips within 30 s and the drug-containing tips were able to release amphotericin B to inhibit the growth of *Candida albicans*.

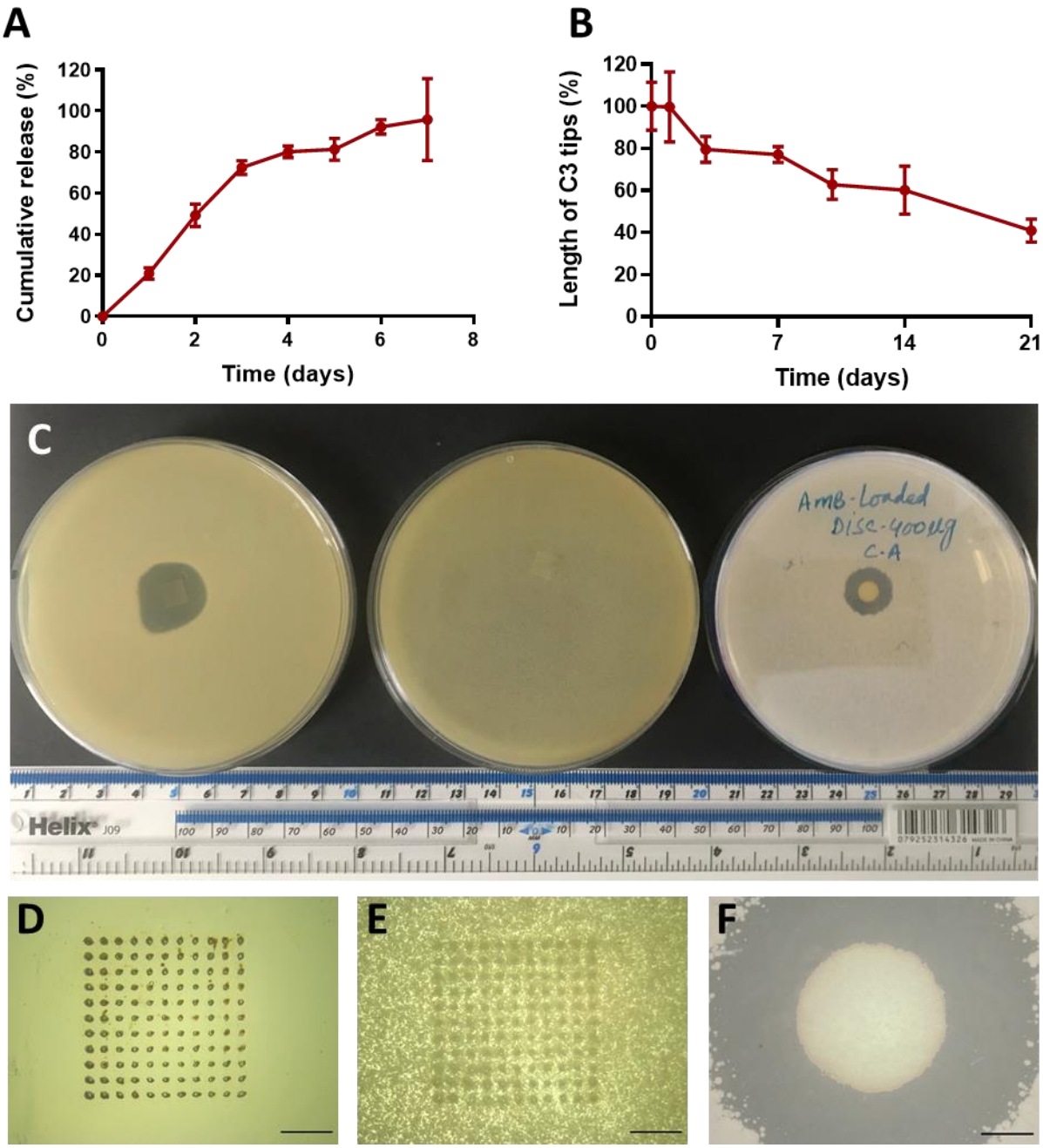

Figure 12. *In vitro* drug release, tip biodegradation and antifungal disk diffusion test results of amphotericin B PLGA C3 tips. (A) *In vitro* drug release profile of amphotericin B PLGA C3 tips. (Means ± SD, n = 5). (B) *In vitro* biodegradation profile of amphotericin B PLGA C3 tips. (Means ± SD, n = 5). (C) Agar plates treated with amphotericin B PLGA-tipped microneedle patches C3-MN8, PVP-tipped microneedle patches, paper disc with 400 µg of amphotericin B; respectively. Microscopic images of the application sites of the agar plates treated with (D) amphotericin B PLGA-tipped microneedle patches C3-MN8, (E) PVP-tipped MN8, and (F) paper disc with 400 µg of amphotericin B. Scale bar, 2 mm.

4. Discussion

Sustained release drug delivery systems are preferred for long-period treatments as a result of improved patient compliance and efficacy [35]. However, surgeries for subcutaneous implantation of the devices or injections into the body are usually required [36,37]. These painful and invasive procedures are generally not able to be self-administrated by patients and, therefore, necessitate the involvement of trained healthcare personnel and the proper handling of biohazard waste. In this work, microneedle technology has been proposed as an alternative delivery method to address these issues.

To develop a tip-implants microneedle system for rapid and efficient drug delivery, PLGA, a biodegradable, FDA-approved material, was chosen as the matrix for the microneedle tips, due to its safety profile, tailored mechanical strength, and extensive application in transdermal drug delivery systems. [38]. The dissolving baseplate was chosen as the literature indicates that it is most commonly used for implantable microneedle system [13–15]. To start with, Nile red, a hydrophobic dye, was delivered as a model compound. The fabrication of this design required castings of hydrophobic polymers (PLGA) and fast dissolvable polymers (PVP), which necessitated separate casting processes. For casting the drug PLGA tips, organic solutions were prepared. The solvents used should dissolve both the drugs and the polymers. TFE was chosen for Nile red PLGA tip solution [39]. The process of casting tips was found to be very important for the fabrication of the system. The length of the PLGA tips can be customized by casting the solution for different replicates.

A key parameter and major concern for implantable microneedle systems is their insertion ability. The insertion ability of the fabricated patches was tested using an artificial film Parafilm M® and porcine skin [7,40]. Parafilm M® presents ductility under external forces, which is an ideal mimic of the *stratum corneum* of the skin. Parafilm M® has been widely used in conjugation with a standard force/time profile as a rapid microneedle insertion quality control test especially for a comparative test of insertion capacities between candidate microneedle formulations [22,25,41,42]. The Parafilm M® insertion study showed the increase of the Nile red PLGA tips might decrease the insertion depth to some extent. Skin insertion was performed for the highest drug loading patch, i.e. C4-MN0 as the means to deliver sufficient amounts of the drug so as to reach the therapeutic window *in vivo*. As shown in the Figure S1 Supplementary Information, the implantation of Nile red PLGA C4 tips was not complete. Even though C4-MN0 was able to penetrate the skin and reached a certain insertion depth, the insertion depth of C4-MN0 was not enough to implant all the tips. The incomplete implantation of C4-MN0 could be attributed to the insertion depth being relatively shallow and the length of tips relatively long. To tackle this issue, two possible alternatives can be explored,

decreasing the length of tips (from C4 to C2) and/or increasing the insertion depth. However, we found the drug delivery efficiency for C2-MN0 was only 39.35% ± 10.01%. Besides, the separation of the PLGA tips from the dissolving baseplate was time consuming (30 min). The dissolution of the dissolving baseplate after 30 min always left a viscous gel on the surface of the skin. As can be observed by the skin insertion and OCT images (Figure 6A1 and 6A2), the incomplete insertion of the tips into the skin caused incomplete drug delivery and a time-consuming separation process.

The insertion depth has been reported to increase with an increase in the length of the needles, thus increasing the delivery efficiency of the formulations loaded in the microneedles [43]. He *et al*. presented the intradermal implantation ratio of microneedle with needle lengths of 500 μm, 600 μm and 700 μm [15]. It was found that microneedles with a length of 500 μm could only deliver about 30% of the implant tips which had a length of 280 μm, while the intradermal implantation ratio of microneedles with lengths of 600 μm and 700 μm could reach 100%. This indicated the increase in the length of the needle could facilitate the intradermal implantation rate of the tips of the needles. It has also been reported that the incorporation of a shaft structure made of materials such as PLA and metal could improve the insertion performance, and facilitate the separation of the tips and the shaft and thus increase the delivery efficiency of the microneedle systems [10,44]. Herein, HFMB cast by Gantrez® S-97 and PEG 200 Da were, for the first time, used as an inert shaft to improve the insertion performance. Two types of HFMB were made, 600 μm-long microneedle base patches (MN6) and 800 μm-long microneedle base patches (MN8). The HFMB was aligned with Nile red PLGA tips as an attempt to increase the delivery efficiency of the system. The alignment of a mechanically strong microneedle base patch could on the one hand increase the mechanical strength of the needles, thus increasing the insertion depth of the system. On the other hand, the increase in the length of the needles would contribute to the increase of insertion depth, thus embedding the PLGA tips inside the skin. Besides, the insertion of the HFMB tips into the hole means that less of the dissolving PVP gel is needed, resulting in less skin interstitial fluid and less time required to separate the PLGA tips from the HFMB once applied into the skin. Such a system enables rapid intradermal delivery of the drug containing tips more quickly and efficiently. Microneedle patches bases with different heights (600 μm and 800 μm) were fabricated. All the patches shared the same interspacing so that HFMB could be aligned into the moulds for fabricating tips. The total needle length after alignment in MN0 based patches was around 600 μm, that in MN6 was around 680 μm and that in MN8 was 970 μm. As the PLGA tips were less than 600 μm, the insertion depths were not required to exceed 600 microns. These insertion depths were ideal as they were sufficient to deposit the PLGA tips, but they are not long enough to generate pain or bleeding [45].

The insertion properties of Nile red PLGA-tipped C2-MN0, C2-MN6, and C2-MN8 patches were tested and compared. *In vitro* insertion tests into the Parafilm M® layers demonstrated that the insertion depth into the Parafilm M® layers increased as with the increase of the needle height of the HFMB, which was in agreement with the literature that the increase of the height needles could increase the insertion depth [10]. The *ex vivo* skin insertion study found that the delivery efficiency increased after alignment with HFMB MN6 or MN8. C2-MN8 implanted 83.72% ± 20.63% of the Nile red inside the patch. Those promising results demonstrated the success of the design.

Amphotericin B is a potent, broad-spectrum antifungal agent, whose application is mainly limited to life-threatening systemic fungal infections due to its systemic side effects. The minimum inhibitory concentration of amphotericin B is generally very low, around 0.5 µg/mL to 1 µg/mL for *Candida albicans* [46]. Topical delivery of long-acting amphotericin B formulations for fungal infections have been preferred because of the avoidance of systemic distribution and thus the avoidance of amphotericin B's notorious nephrotoxicity [47–49]. The implantation of the antifungal therapy will firstly achieve efficient penetration of the antimicrobial agents through the *stratum corneum* into the biofilm. In addition, the drug containing tips will sustain the release of the antimicrobial agent for around a week time, which is highly desirable when continuous drug is exposed at the site of infection [50]. A prolonged and continuous drug exposure at the site of infection is highly desirable for antimicrobial therapy due to reduced toxicity, avoid resistance, administration frequency, dose, and cost [51,52].

Amphotericin B, a typical BCS class IV drug, is hard to administer using conventional topical formulations or oral intake because of its low drug bioavailability to the infection site and lack of sustained therapeutic effect, which might induce antimicrobial resistance [53]. To date, no effective topical products of amphotericin B have been approved by the FDA. Microneedle technologies have made promising progress in the intradermal delivery of amphotericin B. An inkjet-coated Gantrez® AN 169 microneedle patch loading 10.4 µg of amphotericin B has been proposed to combat cutaneous fungal infections. A promising result has been shown in a radial diffusion assay *in vitro* against *Candida parapsilosis* (ATCC 22019) [30]. A poke and patch microneedle system has been explored to deliver amphotericin B in DMSO solution for the treatment of cutaneous *Leishmania*. The antileishmanial results using a *Leishmania Mexicana* challenged murine model showed promise in the intradermal administration of amphotericin B *via* microneedles [54]. Those findings further support the development of an implantable system to deliver amphotericin B intradermally to treat cutaneous fungal infections.

In order to increase drug loading, multiple casting was used to fabricate the amphotericin B PLGA tips. For amphotericin B PLGA-tipped microneedle patches, C3 tips contained 160.0 ± 7.4 µg of amphotericin B. The *in vitro* insertion tests for these patches showed that with the increase of the number of casting replicates, the insertion capacity of the system improved. This was not the case with Nile red PLGA-tipped microneedle patches, where the insertion capability decreased with the increase in the number of casting replicates. This indicated that the properties of the drugs themselves had an impact on the insertion capacity of the microneedles.

The ex vivo skin insertion of amphotericin B PLGA-tipped microneedle patches C3-MN0, C3-MN6, and C3-MN8 was investigated. The delivery efficiency was improved after aligning with MN6 or MN8. Amphotericin B PLGA-tipped C3-MN8 microneedle patches were able to deliver 86.99% ± 11.62% of the drug from the tips into the skin. The release of inserted amphotericin B PLGA C3 tips in PBS containing 1%w/v SLS lasted for 7 days and was fitted well into the zero-order model and the Korsmeyer-Peppas model. *In vitro* disk diffusion test demonstrated the antifungal performance of C3-MN8 against *Candida albicans* NCYC 610.

Unlike PLA, silicon, metal or dodecyl-modified chitosan shafts used in the literature [10,55,56], HFMB MN8 were prepared by crosslinking Gantrez® S-97 and PEG 200 Da to form a hydrogel network. Hydrogels have been extensively used for drug delivery purposes due to their hydrophilic nature and high capability to uptake and retain fluid [57,58]. The swelling capacity of the hydrogels is determined by their crosslinking degree [59]. PEG 200 Da is a low molecular weight crosslinking agent, and thus a highly crosslinked network is obtained. After insertion into the skin, MN8 can absorb the skin interstitial fluid. Upon removal, MN8 was too soft to be reinserted in the skin [60]. In swelling and disintegration studies, the MN8 microneedle base patches were found to have swollen by 106.20% ± 19.39% and disintegrated in water after 15 mins. When exposed to an excess of water, MN8 collapsed and broke. As biohazardous sharp waste remained a burden on public health, as well as the environment [61], the disabled MN8 patches would eliminate needle reuse and be safely disposed of. Furthermore, hydrogel-forming films fabricated using Gantrez® S-97 and PEG 200 Da have been reported to have no adhesion to the porcine skin even in contact with the skin at 5 N for 2 min. This non-adherent property of the materials prevents the risk of dragging the tips from the skin during removal, which is an issue for the dissolving baseplate [60]. These properties made the microneedle base MN8 a perfect fit for enhancing the implantation of the tips and leaving no viscous residue while easy to deal with after use. These properties made the HFMB MN8 a perfect fit for enhancing the implantation of the tips and leaving no viscous residue while being safely disposed of after use as well as eliminating needle reuse [61].

The hybrid microneedle patches designed in this work allowed the self-application of drug-eluting implants. Compared with traditional implants, which requires an invasive surgery process and usually leaves a wound, this novel design would be easy to handle and minimally invasive. Besides, with no drug contained in the base, accurate dosing can be ensured, and waste can be avoided. Additionally, as the HFMB after insertion were too soft to be reinserted and thus can be disposed of safely [62]. Consequently, the proposed system will provide a more convenient and user-friendly option for the long-term delivery of therapeutics.

5. Conclusions

This work produced a hybrid drug containing PLGA-tipped microneedle system for quick implantation of therapeutic substances. Upon insertion into the skin, the drug-containing PLGA tips were embedded in the skin within one minute. Two hydrophobic compounds Nile red and amphotericin B were loaded into the system. An *in vitro* release study demonstrated the release of amphotericin B inside the PLGA tips would last for a week. An antifungal test revealed the effectiveness of the inserted tips against fungal growth. After administration, the HFMB MN8 are non-adhesive to the skin, ensuring easy and complete removal from the skin without any risk of removing the drug loading tips from the skin. Furthermore, after insertion, the HFMB MN8 are too soft and too brittle after immersion in water to be reinserted thus leaving no biohazardous sharp waste. The hybrid patches enable rapid and efficient implantation of therapies to the skin, which simplifies the administration of medications by medical personal or even patients themselves. The results demonstrate that this hybrid patch is a novel promising technology for delivering a drug-eluting implant of hydrophobic drugs.

Acknowledgements

This work was supported by China Scholarship Council and in part by Wellcome Trust grant WT094085MA. We would like to thank Mr Justin O'Hagan from English Language Support, Faculty of Medicine, Health and Life Sciences in Queen's University Belfast for language editing and proofreading this paper.

References

[1] S.A. Stewart, J. Domínguez-Robles, R.F. Donnelly, E. Larrañeta, Implantable polymeric drug delivery devices: Classification, manufacture, materials, and clinical applications, Polymers (Basel). 10 (2018) 1379. https://doi.org/10.3390/polym10121379.

[2] S.A. Stewart, J. Domínguez-Robles, V.J. McIlorum, E. Mancuso, D.A. Lamprou, R.F. Donnelly, E. Larrañeta, Development of a biodegradable subcutaneous implant for prolonged drug delivery using 3D printing, Pharmaceutics. 12 (2020) 105. https://doi.org/10.3390/pharmaceutics12020105.

[3] J.M. Anderson, A. Rodriguez, D.T. Chang, Foreign body reaction to biomaterials, Semin. Immunol. 20 (2008) 86–100. https://doi.org/10.1016/j.smim.2007.11.004.

[4] L.K. Vora, K. Moffatt, I.A. Tekko, A.J. Paredes, F. Volpe-Zanutto, D. Mishra, K. Peng, R. Raj Singh Thakur, R.F. Donnelly, Microneedle array systems for long-acting drug delivery, Eur. J. Pharm. Biopharm. 159 (2021) 44–76. https://doi.org/10.1016/j.ejpb.2020.12.006.

[5] A.S. Rzhevskiy, T.R.R. Singh, R.F. Donnelly, Y.G. Anissimov, Microneedles as the technique of drug delivery enhancement in diverse organs and tissues, J. Control. Release. 270 (2018) 184–202. https://doi.org/10.1016/j.jconrel.2017.11.048.

[6] Á. Cárcamo-Martínez, B. Mallon, J. Domínguez-Robles, L.K. Vora, Q. Kurnia Anjani, R.F. Donnelly, Hollow microneedles: a perspective in biomedical applications, Int. J. Pharm. 599 (2021) 120455. https://doi.org/10.1016/j.ijpharm.2021.120455.

[7] A.H. Sabri, Z. Cater, P. Gurnani, J. Ogilvie, J. Segal, D.J. Scurr, M. Marlow, Intradermal delivery of imiquimod using polymeric microneedles for basal cell carcinoma, Int. J. Pharm. 589 (2020). https://doi.org/10.1016/j.ijpharm.2020.119808.

[8] Á. Cárcamo-Martínez, B. Mallon, Q.K. Anjani, J. Domínguez-Robles, E. Utomo, L.K. Vora, I.A. Tekko, E. Larrañeta, R.F. Donnelly, Enhancing intradermal delivery of tofacitinib citrate: Comparison between powder-loaded hollow microneedle arrays and dissolving microneedle arrays, Int. J. Pharm. 593 (2021) 120152. https://doi.org/10.1016/j.ijpharm.2020.120152.

[9] L. Han, K. Peng, L.-Y. Qiu, M. Li, J.-H. Ruan, L.-L. He, Z.-X. Yuan, Hitchhiking on controlled-release drug delivery systems: Opportunities and challenges for cancer vaccines, Front. Pharmacol. 12 (2021) 1149. https://doi.org/10.3389/fphar.2021.679602.

[10] L.Y. Chu, M.R. Prausnitz, Separable arrowhead microneedles, J. Control. Release. 149 (2011) 242–249. https://doi.org/10.1016/j.jconrel.2010.10.033.

[11] L.K. Vora, R.F. Donnelly, E. Larrañeta, P. González-Vázquez, R.R.S. Thakur, P.R. Vavia, Novel bilayer dissolving microneedle arrays with concentrated PLGA nano-microparticles for targeted intradermal delivery: Proof of concept, J. Control. Release. 265 (2017) 93–101. https://doi.org/10.1016/j.jconrel.2017.10.005.

[12] R.F. Donnelly, E. Larrañeta, Microarray patches: potentially useful delivery systems for long-acting nanosuspensions, Drug Discov. Today. 23 (2018) 1026–1033. https://doi.org/10.1016/j.drudis.2017.10.013.

[13] W. Li, R.N. Terry, J. Tang, M.R. Feng, S.P. Schwendeman, M.R. Prausnitz, Rapidly separable microneedle patch for the sustained release of a contraceptive, Nat. Biomed. Eng. 3 (2019) 220–229. https://doi.org/10.1038/s41551-018-0337-4.

[14] A. Than, K. Liang, S. Xu, L. Sun, H. Duan, F. Xi, C. Xu, P. Chen, Transdermal delivery of anti-obesity compounds to subcutaneous adipose tissue with polymeric microneedle patches, Small Methods. 1 (2017) 1700269. https://doi.org/10.1002/smtd.201700269.

[15] M. He, G. Yang, X. Zhao, S. Zhang, Y. Gao, Intradermal implantable PLGA microneedles for etonogestrel sustained release, J. Pharm. Sci. 109 (2020) 1958–1966. https://doi.org/10.1016/j.xphs.2020.02.009.

[16] D.D. Zhu, Q.L. Wang, X.B. Liu, X.D. Guo, Rapidly separating microneedles for transdermal drug delivery, Acta Biomater. 41 (2016) 312–319. https://doi.org/10.1016/j.actbio.2016.06.005.

[17] J.G. Turner, L.R. White, P. Estrela, H.S. Leese, Hydrogel-forming microneedles: Current advancements and future trends, Macromol. Biosci. 21 (2021) 2000307. https://doi.org/10.1002/mabi.202000307.

[18] I.A. Tekko, G. Chen, J. Domínguez-Robles, R.R.S. Thakur, I.M.N. Hamdan, L. Vora,

E. Larrañeta, J.C. McElnay, H.O. McCarthy, M. Rooney, R.F. Donnelly, Development and characterisation of novel poly (vinyl alcohol)/poly (vinyl pyrrolidone)-based hydrogel-forming microneedle arrays for enhanced and sustained transdermal delivery of methotrexate, Int. J. Pharm. 586 (2020) 119580. https://doi.org/10.1016/j.ijpharm.2020.119580.

[19] C.W. Peak, J.J. Wilker, G. Schmidt, A review on tough and sticky hydrogels, Colloid Polym. Sci. 291 (2013) 2031–2047. https://doi.org/10.1007/s00396-013-3021-y.

[20] Á. Cárcamo-Martínez, Q.K. Anjani, A.D. Permana, A.S. Cordeiro, E. Larrañeta, R.F. Donnelly, Coated polymeric needles for rapid and deep intradermal delivery, Int. J. Pharm. X. 2 (2020) 100048. https://doi.org/10.1016/j.ijpx.2020.100048.

[21] E. Larrañeta, S. Stewart, S.J. Fallows, L.L. Birkhäuer, M.T.C. McCrudden, A.D. Woolfson, R.F. Donnelly, A facile system to evaluate in vitro drug release from dissolving microneedle arrays, Int. J. Pharm. 497 (2016) 62–69. https://doi.org/10.1016/j.ijpharm.2015.11.038.

[22] E. Larrañeta, J. Moore, E.M. Vicente-Pérez, P. González-Vázquez, R. Lutton, A.D. Woolfson, R.F. Donnelly, A proposed model membrane and test method for microneedle insertion studies, Int. J. Pharm. 472 (2014) 65–73. https://doi.org/10.1016/j.ijpharm.2014.05.042.

[23] L.K. Vora, P.R. Vavia, E. Larrañeta, S.E.J. Bell, R.F. Donnelly, Novel nanosuspension-based dissolving microneedle arrays for transdermal delivery of a hydrophobic drug, J. Interdiscip. Nanomedicine. 3 (2018) 89–101. https://doi.org/10.1002/jin2.41.

[24] A. Summerfield, F. Meurens, M.E. Ricklin, The immunology of the porcine skin and its value as a model for human skin, Mol. Immunol. 66 (2015) 14–21. https://doi.org/10.1016/j.molimm.2014.10.023.

[25] L.K. Vora, A.J. Courtenay, I.A. Tekko, E. Larrañeta, R.F. Donnelly, Pullulan-based dissolving microneedle arrays for enhanced transdermal delivery of small and large biomolecules, Int. J. Biol. Macromol. 146 (2020) 290–298. https://doi.org/10.1016/j.ijbiomac.2019.12.184.

[26] R.F. Donnelly, M.J. Garland, D.I.J. Morrow, K. Migalska, T.R.R. Singh, R. Majithiya,

A.D. Woolfson, Optical coherence tomography is a valuable tool in the study of the effects of microneedle geometry on skin penetration characteristics and in-skin dissolution, J. Control. Release. 147 (2010) 333–341. https://doi.org/10.1016/j.jconrel.2010.08.008.

[27] P. Costa, J.M. Sousa Lobo, Modeling and comparison of dissolution profiles, Eur. J. Pharm. Sci. 13 (2001) 123–133. https://doi.org/10.1016/S0928-0987(01)00095-1.

[28] E. Larrañeta, C. Martínez-Ohárriz, I. Vélaz, A. Zornoza, R. Machín, J.R. Isasi, In vitro release from reverse poloxamine/α-Cyclodextrin matrices: Modelling and comparison of dissolution profiles, J. Pharm. Sci. 103 (2014) 197–206. https://doi.org/10.1002/jps.23774.

[29] Y. Zhang, M. Huo, J. Zhou, A. Zou, W. Li, C. Yao, S. Xie, DDSolver: An add-in program for modeling and comparison of drug dissolution profiles, AAPS J. 12 (2010) 263–271. https://doi.org/10.1208/s12248-010-9185-1.

[30] R.D. Boehm, P.R. Miller, W.A. Schell, J.R. Perfect, R.J. Narayan, Inkjet printing of amphotericin B onto biodegradable microneedles using piezoelectric inkjet printing, JOM. 65 (2013) 525–533. https://doi.org/10.1007/s11837-013-0574-7.

[31] International conference on harmonisation of technical requirements for registration of pharmaceuticals for human use, ICH Harmonised Tripartite Guideline - Validation of Analytical Procedures: Text and Methodology Q2 (R1), 2005.

[32] L.K. Vora, P.R. Vavia, E. Larrañeta, S.E.J. Bell, R.F. Donnelly, Novel nanosuspension-based dissolving microneedle arrays for transdermal delivery of a hydrophobic drug, J. Interdiscip. Nanomedicine. 3 (2018) 89–101. https://doi.org/10.1002/jin2.41.

[33] D.F. de Souza, K. Goebel, I.F. Andreazza, Development of enteric coated sustained release minitablets containing mesalamine, Brazilian J. Pharm. Sci. 49 (2013) 529–536. https://doi.org/10.1590/S1984-82502013000300014.

[34] M. Padmaa Paarakh, P. Ani Jose, C.M. Setty, G.V.P. Christoper, Release kinetics - concepts and applications, Int. J. Pharm. Res. Technol. 8 (2018) 12–20.

[35] K.B. Sutradhar, C.D. Sumi, Implantable microchip: the futuristic controlled drug

delivery system, Drug Deliv. 23 (2016) 1–11. https://doi.org/10.3109/10717544.2014.903579.

[36] K. Peng, C. Wu, G. Wei, J. Jiang, Z. Zhang, X. Sun, Implantable sandwich PHBHHx film for burst-free controlled delivery of thymopentin peptide, Acta Pharm. Sin. B. 8 (2018) 432–439. https://doi.org/https://doi.org/10.1016/j.apsb.2018.03.003.

[37] L. Han, J. Xue, L. Wang, K. Peng, Z. Zhang, T. Gong, X. Sun, An injectable, low-toxicity phospholipid-based phase separation gel that induces strong and persistent immune responses in mice, Biomaterials. 105 (2016) 185–194. https://doi.org/10.1016/j.biomaterials.2016.08.007.

[38] S. Li, Y. chun Zeng, K. Peng, C. Liu, Z. rong Zhang, L. Zhang, Design and evaluation of glomerulus mesangium-targeted PEG-PLGA nanoparticles loaded with dexamethasone acetate, Acta Pharmacol. Sin. 40 (2019) 143–150. https://doi.org/10.1038/s41401-018-0052-4.

[39] Y.L. Ji, P.S. Wolfe, I.A. Rodriguez, G.L. Bowlin, Preparation of chitin nanofibril/polycaprolactone nanocomposite from a nonaqueous medium suspension, Carbohydr. Polym. 87 (2012) 2313–2319. https://doi.org/10.1016/j.carbpol.2011.10.066.

[40] A.H. Sabri, Y. Kim, M. Marlow, D.J. Scurr, J. Segal, A.K. Banga, L. Kagan, J.B. Lee, Intradermal and transdermal drug delivery using microneedles – Fabrication, performance evaluation and application to lymphatic delivery, Adv. Drug Deliv. Rev. 153 (2020) 195–215. https://doi.org/10.1016/j.addr.2019.10.004.

[41] C. Yeung, S. Chen, B. King, H. Lin, K. King, F. Akhtar, G. Diaz, B. Wang, J. Zhu, W. Sun, A. Khademhosseini, S. Emaminejad, A 3D-printed microfluidic-enabled hollow microneedle architecture for transdermal drug delivery, Biomicrofluidics. 13 (2019) 064125. https://doi.org/10.1063/1.5127778.

[42] P. González-Vázquez, E. Larrañeta, M.T.C. McCrudden, C. Jarrahian, A. Rein-Weston, M. Quintanar-Solares, D. Zehrung, H. McCarthy, A.J. Courtenay, R.F. Donnelly, Transdermal delivery of gentamicin using dissolving microneedle arrays for potential treatment of neonatal sepsis, J. Control. Release. 265 (2017) 30–40.

https://doi.org/10.1016/j.jconrel.2017.07.032.

[43] L.C. Su, M.C. Chen, Efficient delivery of nanoparticles to deep skin layers using dissolvable microneedles with an extended-length design, J. Mater. Chem. B. 5 (2017) 3355–3363. https://doi.org/10.1039/c7tb00451f.

[44] D.D. Zhu, Q.L. Wang, X.B. Liu, X.D. Guo, Rapidly separating microneedles for transdermal drug delivery, Acta Biomater. 41 (2016) 312–319. https://doi.org/10.1016/j.actbio.2016.06.005.

[45] H.S. Gill, D.D. Denson, B.A. Burris, M.R. Prausnitz, Effect of microneedle design on pain in human volunteers, Clin. J. Pain. 24 (2008) 585–594. https://doi.org/10.1097/AJP.0b013e31816778f9.

[46] M.E. Klepser, E.J. Wolfe, R.N. Jones, C.H. Nightingale, M.A. Pfaller, Antifungal pharmacodynamic characteristics of fluconazole and amphotericin B tested against Candida albicans, Antimicrob. Agents Chemother. 41 (1997) 1392–1395. https://doi.org/10.1128/aac.41.6.1392.

[47] A. Hussain, A. Samad, S.K. Singh, M.N. Ahsan, M.W. Haque, A. Faruk, F.J. Ahmed, Nanoemulsion gel-based topical delivery of an antifungal drug: In vitro activity and in vivo evaluation, Drug Deliv. 23 (2016) 652–667. https://doi.org/10.3109/10717544.2014.933284.

[48] G. Roy, R.D. Galigama, V.S. Thorat, L.S. Mallela, S. Roy, P. Garg, V.V.K. Venuganti, Amphotericin B containing microneedle ocular patch for effective treatment of fungal keratitis, Int. J. Pharm. 572 (2019) 118808. https://doi.org/10.1016/j.ijpharm.2019.118808.

[49] S. Güngör, M.S. Erdal, B. Aksu, New formulation strategies in topical antifungal therapy, J. Cosmet. Dermatological Sci. Appl. 03 (2013) 56–65. https://doi.org/10.4236/jcdsa.2013.31a009.

[50] R. Jamaledin, C.K.Y. Yiu, E.N. Zare, L.N. Niu, R. Vecchione, G. Chen, Z. Gu, F.R. Tay, P. Makvandi, Advances in antimicrobial microneedle patches for combating infections, Adv. Mater. 32 (2020) 2002129. https://doi.org/10.1002/adma.202002129.

[51] F.W.M. da S. de Bastiani, C. de C. Spadari, J.K.R. de Matos, G.C. Salata, L.B. Lopes, K. Ishida, Nanocarriers provide sustained antifungal activity for amphotericin B and miltefosine in the topical treatment of murine vaginal Candidiasis, Front. Microbiol. 10 (2020) 2976. https://doi.org/10.3389/fmicb.2019.02976.

[52] F. Volpe-Zanutto, L.T. Ferreira, A.D. Permana, M. Kirkby, A.J. Paredes, L.K. Vora, A. P. Bonfanti, I. Charlie-Silva, C. Raposo, M.C. Figueiredo, I.M.O. Sousa, A. Brisibe, F.T.M. Costa, R.F. Donnelly, M.A. Foglio, Artemether and lumefantrine dissolving microneedle patches with improved pharmacokinetic performance and antimalarial efficacy in mice infected with Plasmodium yoelii, J. Control. Release. 333 (2021) 298–315. https://doi.org/10.1016/j.jconrel.2021.03.036.

[53] P. Zan, A. Than, P.K. Duong, J. Song, C. Xu, P. Chen, Antimicrobial microneedle patch for treating deep cutaneous fungal infection, Adv. Ther. 2 (2019) 1900064. https://doi.org/10.1002/adtp.201900064.

[54] A.K. Nguyen, K.H. Yang, K. Bryant, J. Li, A.C. Joice, K.A. Werbovetz, R.J. Narayan, Microneedle-based delivery of amphotericin B for treatment of cutaneous Leishmaniasis, Biomed. Microdevices. 21 (2019). https://doi.org/10.1007/s10544-018-0355-8.

[55] A. Vrdoljak, M.G. McGrath, J.B. Carey, S.J. Draper, A.V.S. Hill, C. O'Mahony, A.M. Crean, A.C. Moore, Coated microneedle arrays for transcutaneous delivery of live virus vaccines, J. Control. Release. 159 (2012) 34–42. https://doi.org/10.1016/j.jconrel.2011.12.026.

[56] X. Zhang, G. Chen, L. Cai, Y. Wang, L. Sun, Y. Zhao, Bioinspired pagoda-like microneedle patches with strong fixation and hemostasis capabilities, Chem. Eng. J. 414 (2021) 128905. https://doi.org/10.1016/j.cej.2021.128905.

[57] L.A. Sharpe, A.M. Daily, S.D. Horava, N.A. Peppas, Therapeutic applications of hydrogels in oral drug delivery, Expert Opin. Drug Deliv. 11 (2014) 901–915. https://doi.org/10.1517/17425247.2014.902047.

[58] E. Larrañeta, J.R. Isasi, Non-covalent hydrogels of cyclodextrins and poloxamines for the controlled release of proteins, Carbohydr. Polym. 102 (2014) 674–681. https://doi.org/10.1016/j.carbpol.2013.11.002.

[59] S.H. Khalid, M.I. Qadir, A. Massud, M. Ali, M.H. Rasool, Effect of degree of cross-linking on swelling and drug release behaviour of poly(methyl methacrylate-co-itaconic acid) [P(MMA/IA)] hydrogels for site specific drug delivery, J. Drug Deliv. Sci. Technol. 19 (2009) 413–418. https://doi.org/10.1016/S1773-2247(09)50085-8.

[60] Á. Cárcamo-Martínez, J. Domínguez-Robles, B. Mallon, M.T. Raman, A.S. Cordeiro, S.E.J. Bell, E. Larrañeta, R.F. Donnelly, Potential of polymeric films loaded with gold nanorods for local hyperthermia applications, Nanomaterials. 10 (2020) 582. https://doi.org/10.3390/nano10030582.

[61] B. Sapkota, G.K. Gupta, D. Mainali, Impact of intervention on healthcare waste management practices in a tertiary care governmental hospital of Nepal, BMC Public Health. 14 (2014) 1–8. https://doi.org/10.1186/1471-2458-14-1005.

[62] A.R.J. Hutton, H.L. Quinn, P.J. McCague, C. Jarrahian, A. Rein-Weston, P.S. Coffey, E. Gerth-Guyette, D. Zehrung, E. Larrañeta, R.F. Donnelly, Transdermal delivery of vitamin K using dissolving microneedles for the prevention of vitamin K deficiency bleeding, Int. J. Pharm. 541 (2018) 56–63. https://doi.org/10.1016/j.ijpharm.2018.02.031.